A non-linear consolidation theory for soils exhibiting secondary compression

Gilberto Alexandre, Luciana Thomasi

A Non-linear Consolidation Theory for Soils Exhibiting Secondary Compression

Gilberto Alexandre, PhD, P.Eng
gilberto.alexandre@saskpolytech.ca

Luciana Thomasi, M.Sc, P.Eng
lthomasi@yahoo.ca

February 9, 2023

Abstract

In this paper a non-linear theory for the consolidation of saturated soils under vertical deformation and flow accounting for secondary compression is developed. The theory builds on the work of Gibson and Lo (1961) [1] but, instead of using a linear dashpot, adopts either a power law or a logarithmic viscous function for the representation of the structural viscosity of the soil. The new theory is then assessed having as comparison conventional test results from Taylor (1948) [2] and results of long-term consolidation tests as reported in Carvalho (1997) [3]. Very good agreement between estimated behaviour and experimental results suggests the potential of the new theory.

1 Introduction

Gibson and Lo (1961) presented a consolidation theory for soils exhibiting secondary compression that can be seen as a rheological model made of a linear spring in series with a linear Kelvin-Voigt body. In this theory the spring that is connected to the Kelvin-Voigt body represents the transient deformation and flow of the consolidation process while the Kelvin-Voigt body represents secondary compression with its structural viscous resistance to compression of the soil. For this rheological model the authors were able to derive a differential equation and obtain its closed form solution which

shows, in addition to the well-known transient flow and deformation process, the secondary compression that is observed in consolidation tests. Despite the great advance this theory represents, there is significant evidence that the viscous behaviour of soils is non-linear as can be seen in, for example, Leroueil (1985) [4], Martins (1992) [5], Alexandre (2006) [6] and Alexandre(2017) [7]. It is, therefore, conjectured that replacing the linear dashpot by a suitable non-linear function could perhaps lead to better agreement with the actual observed behaviour of soils regarding secondary compression. This is, therefore, the goal of the new theory presented in this paper.

This new rheological model, for which the differential equations will be presented in the section that follows is represented in Figure 1 below:

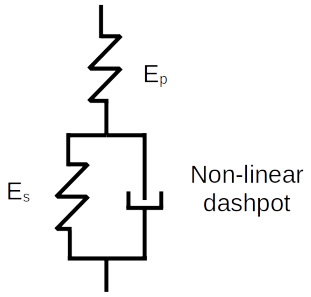

Figure 1: Rheological model adopted in the new theory.

2 The Differential Equations

The starting point of the differential equations developed in this paper is the well-known equation from Terzaghi's consolidation theory:

$$\frac{k}{\gamma_w} \cdot \frac{\partial^2 u}{\partial z^2} = -\frac{\partial \epsilon}{\partial t} \tag{1}$$

In Equation 1 above, k is the permeability of the soil, γ_w is the unit weight of the water, u is the excess pore-pressure, z is the vertical coordinate along the soil layer, ϵ is the vertical (or axial) strain and t is the time.

Since $\sigma^{'} = \sigma - u$ and assuming that total stresses are constant over depth (or, at most, vary linearly with depth), if follows that:

$$\frac{k}{\gamma_w} \cdot \frac{\partial^2 \sigma^{'}}{\partial z^2} = \frac{\partial \epsilon}{\partial t} \tag{2}$$

This equation is, of course, equivalent to the one which is the starting point of the derivation given in Gibson and Lo (1961). The only difference between these equations is that, in the present paper, vertical strain is used instead of void ratio.

The total strain experienced by the soil element is, in accordance to the present model (as it is also in theory from Gibson and Lo, 1961), the sum of the strain from primary consolidation and the strain from secondary compression. Therefore:

$$\epsilon = \epsilon_p + \epsilon_s \tag{3}$$

Where ϵ_p is the strain from primary consolidation, represented by the linear spring in series with the Kelvin-Voigt body and ϵ_s is the strain from secondary compression, represented by the second spring in the Kelvin-Voigt body. Substituting the first partial derivative of Equation 3 with respect to time in Equation 2 gives:

$$\frac{k}{\gamma_w} \cdot \frac{\partial^2 \sigma^{'}}{\partial z^2} = \frac{\partial \epsilon_p}{\partial t} + \frac{\partial \epsilon_s}{\partial t} \tag{4}$$

Considering that for primary consolidation $\sigma^{'} = E_p \cdot \epsilon_p$, where E_p is the oedometric modulus for primary consolidation, and assuming a constant E_p, then Equation 4 can be re-written as:

$$\frac{k}{\gamma_w} \cdot \frac{\partial^2 \sigma^{'}}{\partial z^2} = \frac{1}{E_p} \cdot \frac{\partial \sigma^{'}}{\partial t} + \frac{\partial \epsilon_s}{\partial t} \tag{5}$$

The last component of the differential equation is about an expression for $\frac{\partial \epsilon_s}{\partial t}$, which in turn, is related to the interaction between the linear spring from primary consolidation and the Kelvin-Voigt body. This interaction, on the other hand, depends on the properties of the spring and of the dashpot on the Kelvin-Voigt body. If, for example, it is assumed a linear spring,

represented by the oedometric modulus for secondary compression, E_s, and a linear dashpot, represented by a constant viscosity coefficient, η, then:

$$\sigma^{'} = E_s \cdot \epsilon_s + \eta \cdot \frac{\partial \epsilon_s}{\partial t} \tag{6}$$

Solving Equation 6 for the strain rate due to secondary compression and substituting in Equation 5 gives:

$$\frac{k}{\gamma_w} \cdot \frac{\partial^2 \sigma^{'}}{\partial z^2} = \frac{1}{E_p} \cdot \frac{\partial \sigma^{'}}{\partial t} + \frac{\sigma^{'} - E_s \cdot \epsilon_s}{\eta} \tag{7}$$

Again, it can be shown that Equation 7 is equivalent to the theory developed by Gibson and Lo (1961). However, if a non-linear dashpot represented by $\sigma_{visc} = K \cdot \frac{\partial \epsilon_s}{\partial t}^{n}$ is used (where σ_{visc} is the viscous resistance to compression of the soil), then the differential equation becomes:

$$\frac{k}{\gamma_w} \cdot \frac{\partial^2 \sigma^{'}}{\partial z^2} = \frac{1}{E_p} \cdot \frac{\partial \sigma^{'}}{\partial t} + \left[\frac{\sigma^{'} - E_s \cdot \epsilon_s}{K}\right]^{1/n} \tag{8}$$

As illustrated by Equations 7 and 8, a unique differential equation is created just by selecting a suitable expression for the strain rate during secondary compression. One empirical equation for the representation of the viscous resistance of soils, which was found to work well for the representation of the stress relaxation of the reconstituted *Onsöy* clay, as reported by Alexandre (2017) is $\sigma_{visc} = B + A \cdot \ln(C \cdot \frac{\partial \epsilon_s}{\partial t})$, where A, B and C are constants. Using this logarithmic function, the differential equation becomes:

$$\frac{k}{\gamma_w} \cdot \frac{\partial^2 \sigma^{'}}{\partial z^2} = \frac{1}{E_p} \cdot \frac{\partial \sigma^{'}}{\partial t} + \frac{e^{\left(\frac{\sigma^{'} - E_s \cdot \epsilon_s - B}{A}\right)}}{C} \tag{9}$$

3 Numerical Procedure

Equations 7, 8 and 9 can be solved by the following respective finite differences schemes:

$$\sigma^{'}_{i,t+\Delta t} = E_p{\cdot}\Delta t \left[\frac{\sigma^{'}_{i,t}}{E_p \cdot \Delta t} - \left(\frac{\sigma^{'}_{i,t} - E_s \cdot \epsilon_{s(i,t)}}{\eta} \right) + \frac{k}{\gamma_w} \cdot \left(\frac{\sigma^{'}_{i-1,t} + \sigma^{'}_{i+1,t} - 2 \cdot \sigma^{'}_{i,t}}{\Delta z^2} \right) \right] \tag{10}$$

$$\sigma^{'}_{i,t+\Delta t} = E_p{\cdot}\Delta t \left[\frac{\sigma^{'}_{i,t}}{E_p \cdot \Delta t} - \left(\frac{\sigma^{'}_{i,t} - E_s \cdot \epsilon_{s(i,t)}}{K} \right)^{1/n} + \frac{k}{\gamma_w} \cdot \left(\frac{\sigma^{'}_{i-1,t} + \sigma^{'}_{i+1,t} - 2 \cdot \sigma^{'}_{i,t}}{\Delta z^2} \right) \right] \tag{11}$$

$$\sigma^{'}_{i,t+\Delta t} = E_p{\cdot}\Delta t \left[\frac{\sigma^{'}_{i,t}}{E_p \cdot \Delta t} - \frac{e^{\left(\frac{\sigma^{'}_{i,t} - E_s \cdot \epsilon_{s(i,t)} - B}{A} \right)}}{C} + \frac{k}{\gamma_w} \cdot \left(\frac{\sigma^{'}_{i-1,t} + \sigma^{'}_{i+1,t} - 2 \cdot \sigma^{'}_{i,t}}{\Delta z^2} \right) \right] \tag{12}$$

In Equations 10, 11 and 12, Δz and Δt represent the spatial and time discretizations, respectively.

These equations differ only in the term used for calculating the strain rate from the secondary compression, which, in turn, is unique for each different Kelvin-Voigt body. As such, the description of the numerical procedure for one of these equations is directly applicable to the other two.

A simple inspection of these equations reveals that the determination of $\sigma^{'}_{i,t+\Delta t}$ depends only on the values of vertical effective stresses at this point and two adjacent points as well as on the value of the secondary compression strain at this point from a previous time-step. It is then sufficient only to know the initial and boundary conditions for obtaining the complete description of stresses, strains, excess pore-pressures and other variables of interest at any given time.

The initial and boundary conditions in the present theory are equivalent to their respective counterparts in Terzaghi's theory. That is:

- For $z = 0$ and for $z = 2H$, $u = 0$, which in turn means that $\sigma^{'} = \Delta\sigma$ at the "drainage boundaries"; and
- For $t = 0$, $u = u_i$, (u_i is the initial excess pore-pressure distribution), which in turn means that $\sigma^{'} = 0$ along the entire soil layer.

It is important to note that $\sigma^{'}$ represents, in this context, the gain or the increase in the vertical effective stresses during the process. Since at

$t = 0$ the gain/increase in vertical effective stresses is zero then it is clear that both primary consolidation strains and secondary compression strains are also zero at this point in time.

With these initial and boundary conditions, the appropriate equation (10, 11 or 12) and with a suitable spatial and time discretization, the problem can be solved satisfactorily. In relation to the marching in time, the following conventional approximation is used:

$$\epsilon_s(i, t + \Delta t) \approx \epsilon_s(i, t) + \frac{\partial \epsilon_s}{\partial t}(i, t) \cdot \Delta t \tag{13}$$

That said, when using Equation 12, care is required when calculating the secondary compression strain rate. This is the result of using the logarithmic viscous function, $\sigma_{visc} = B + A \cdot \ln(C \cdot \frac{\partial \epsilon_s}{\partial t})$. This function is not defined for zero strain rate, which means that the viscous resistance to compression will drop to zero for a strain rate greater than zero (although typically this strain rate is very small). This problem, however, can be addressed in programming by making the strain rate equal to zero whenever its calculated value reaches or is below $\frac{e^{\frac{-B}{A}}}{C}$.

3.1 Approximate Numerical Procedure

The full numerical procedure as described above requires solving the differential equations by a finite differences scheme along the depth of the entire layer over time. As such, this procedure requires programming, which although straightforward in comparison to more sophisticated numerical methods like the Finite Element Method, is more laborious than using a spreadsheet.

As it will be seen in this section, there is an alternative which is much simpler than the full numerical procedure mentioned above. This approximate numerical procedure was found to give very good results in all the comparisons made in this paper and can be implemented with a spreadsheet.

The approximate procedure consists in treating the problem on average terms. That is, the spring that is connected to the Kelvin-Voigt body, which represents the transient flow and deformation of the soil layer, is at the same time, the loading acting on the Kelvin-Voigt body. As such, the problem can be represented, on average, by the following equations below, depending on which of the three rheological models presented above is used:

$$\bar{\sigma}'(t) = E \cdot \bar{\epsilon}_s + \eta \cdot \frac{d\bar{\epsilon}_s}{dt} \tag{14}$$

$$\bar{\sigma}^{'}(t) = E \cdot \bar{\epsilon}_s + K \cdot \frac{d\bar{\epsilon}_s}{dt}^n \tag{15}$$

$$\bar{\sigma}^{'}(t) = E \cdot \bar{\epsilon}_s + B + A \cdot \ln\left(C \cdot \frac{d\bar{\epsilon}_s}{dt}\right) \tag{16}$$

Knowing the "loading", $\bar{\sigma}^{'}(t)$, allows us to calculate the average strain rate as:

$$\frac{d\bar{\epsilon}_s}{dt} = \frac{\bar{\sigma}^{'}(t) - E \cdot \bar{\epsilon}_s}{\eta} \tag{17}$$

$$\frac{d\bar{\epsilon}_s}{dt} = \left[\frac{\bar{\sigma}^{'}(t) - E \cdot \bar{\epsilon}_s}{K}\right]^{\frac{1}{n}} \tag{18}$$

$$\frac{d\bar{\epsilon}_s}{dt} = \frac{1}{C} \cdot e^{\left[\frac{\bar{\sigma}^{'}(t) - E \cdot \bar{\epsilon}_s - B}{A}\right]} \tag{19}$$

To simplify further the procedure, empirical equations for the average degree of consolidation can be used to approximate the Fourier series from Terzaghi's solution. In this paper, the approximation suggested by Brinch-Hansen (1961) [8], reproduced below, will be used:

$$\bar{U} = \sqrt[6]{\frac{T_v^3}{T_v^3 + 0.5}} \tag{20}$$

Where T_v is the time factor from Terzaghi's theory. With the "loading" given by $\bar{\sigma}^{'}(t) = \bar{U} \cdot \Delta\sigma$, the approximate step-by-step procedure becomes:

- At time $t = 0$, $\bar{\sigma}^{'}(0) = 0$ and $\bar{\epsilon}_s = 0$. Therefore $\frac{d\bar{\epsilon}_s}{dt} = 0$;
- A moment later, at time $(t + \Delta t)$, $\bar{U} = \sqrt[6]{\frac{T_v^3(t+\Delta t)}{T_v^3(t+\Delta t)+0.5}}$, $\bar{\sigma}^{'}(t) = \bar{U}(t + \Delta t) \cdot \Delta\sigma$ and the average secondary compression strain rate can be calculated using Equations 17, 18 or 19;
- The average axial strain from secondary compression can then be calculated as $\epsilon_s(t + \Delta t) \approx \bar{\epsilon}_s(t) + \frac{d\bar{\epsilon}_s}{dt}(t) \cdot \Delta t$; and
- The average axial strain can be calculated as $\bar{\epsilon} = \bar{\epsilon}_p + \bar{\epsilon}_s$ where $\bar{\epsilon}_p = \frac{\bar{\sigma}^{'}(t)}{E_p}$

4 Assessment of Parametres

Since the present approach is numerical and the consolidation process accounting for secondary compression is gradual over time and varies along the depth of the soil layer, the estimation of the required soil parametres becomes difficult.

Despite this problem, a first approximation can be made having in mind the interaction between the linear spring and the non-linear Kelvin-Voigt body. As the spring represents the transient nature of the water flow and deformation of the soil layer and is, at the same time, the loading acting on the Kelvin-Voigt body, it is clear that secondary compression is activated by primary consolidation. And since this loading increases gradually from zero to $\Delta\sigma$ over time and along the depth of the soil layer, it can be argued that, in the laboratory at the beginning of the process, the deformation due to the transient water flow process prevails over the deformation due to the structural viscous resistance to compression. That is, primary consolidation dominates the beginning of the process. If this is the case, then the parametres related to primary consolidation can be estimated using Taylor's method.

By the same token, it seems reasonable to assume that the deformation due to the structural resistance to compression dominates the later portion of the process. Therefore, the parametres of the viscous function can be estimated as if the transient water flow and deformation had little influence on the later stage of the process. In other words, the viscous parametres can be estimated assuming the entire soil specimen as behaving uniformingly in accordance with the Kelvin-Voigt body.

With this guidance, the following step-by-step procedure, which was used in this paper, is suggested:

- Determine the vertical coefficient of consolidation, c_v using Taylor's method;
- Estimate the end of primary strain, $\bar{\epsilon}_{100}$, as $\bar{\epsilon}_{100} = (10/9) \cdot \bar{\epsilon}_{90}$, where $\bar{\epsilon}_{90}$ is the strain at ninety percent average degree of consolidation;
- Calculate $E_p = \Delta\sigma/\bar{\epsilon}_{100}$;
- Estimate the final strain, $\bar{\epsilon}_f$;
- Calculate $E_s = \Delta\sigma/(\bar{\epsilon}_f - \bar{\epsilon}_{100})$;

- Choose two (or more) points in the secondary tail of the consolidation curve; and
- For these two (or more) points:

  - Determine their respective strains and strain rates. Say, for example, for points $\bar{\epsilon}_1$, $\bar{\epsilon}_2$, etc.;

  - Determine the average viscous resistance to compression as $\bar{\sigma}_{visc,1} = E_s \cdot (\bar{\epsilon}_f - \bar{\epsilon}_1)$, $\bar{\sigma}_{visc,2} = E_s \cdot (\bar{\epsilon}_f - \bar{\epsilon}_2)$, etc.;

  - Determine the viscous parametres (either A and B or K and n) using the pair of values $(\frac{d\bar{\epsilon}_s}{dt}, \bar{\sigma}_{visc})$.

The procedure above described is the same regardless if the finite differences or the approximate procedure is used.

5 Comparison with the Tests from Taylor (1948)

In this section, the new theory is applied to the results of a conventional consolidation test carried out in a clay from Chicago and reported in Taylor (1948). The same tabulated data from Taylor (1948) can also be found in the book by Holtz and Kovacs (1981) [9].

For each loading increment, a table with all the estimate parametres is provided as well as a plot of the estimated viscous functions (for both a power law and a logarithmic function, each with their respective correlation coefficient, R^2) and a plot showing the test data and predictions.

5.1 Loading Increment №1

Parametre	Estimated value
$\Delta\sigma(kPa)$	12.3
$\bar{\epsilon}_{90}$	0.00245
$\bar{\epsilon}_{100}$	0.00272
$\bar{\epsilon}_f$	0.0045
$t_{90}(s)$	676
$E_p(kPa)$	4,503
$E_s(kPa)$	6,896
$c_v(\frac{m^2}{s})$	3.17×10^{-7}
$k(m/s)$	6.91×10^{-10}

Table 1: Summary table

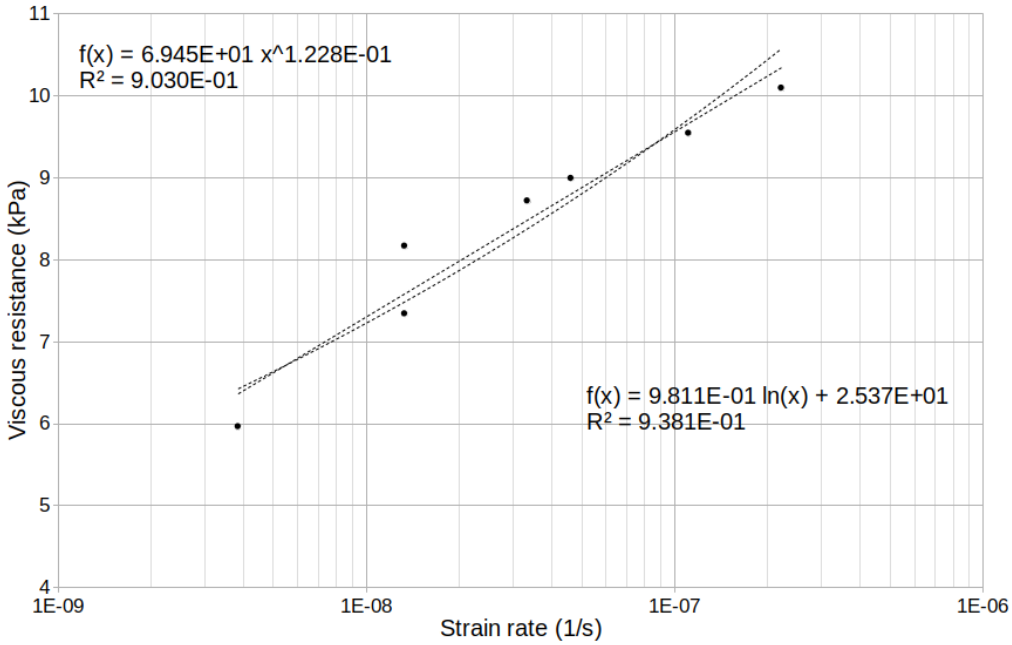

Figure 2: Estimated viscous functions.

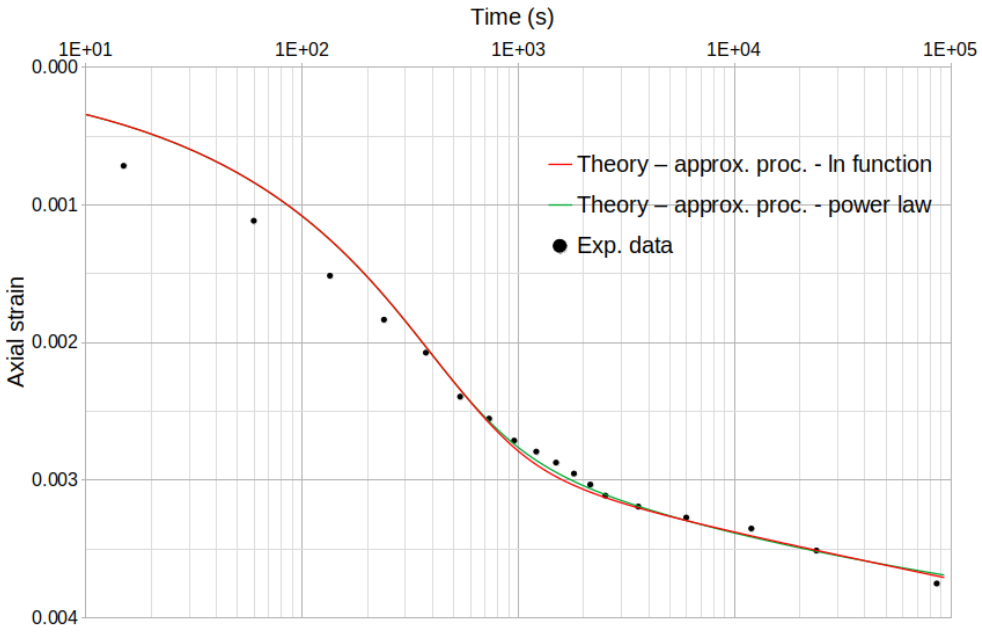

Figure 3: Experimental data and predictions.

5.2 Loading Increment №2

Parametre	Estimated value
$\Delta\sigma(kPa)$	24.5
$\bar{\epsilon}_{90}$	0.0059
$\bar{\epsilon}_{100}$	0.00656
$\bar{\epsilon}_f$	0.009
$t_{90}(s)$	1,156
$E_p(kPa)$	3,740
$E_s(kPa)$	10,030
$c_v(\frac{m^2}{s})$	1.83×10^{-7}
$k(m/s)$	4.80×10^{-10}

Table 2: Summary table

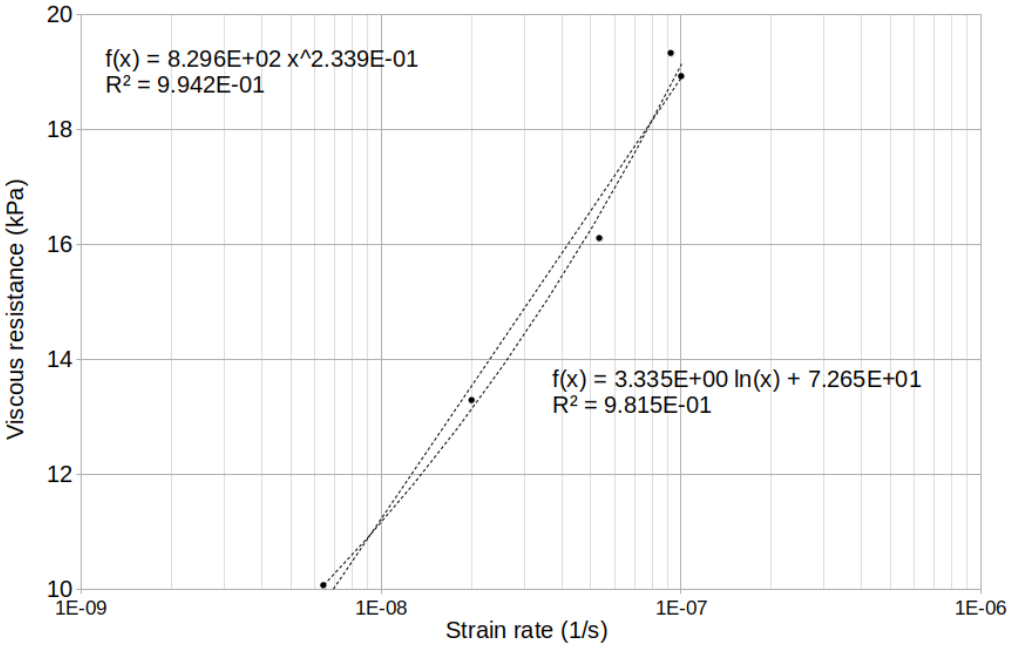

Figure 4: Estimated viscous functions.

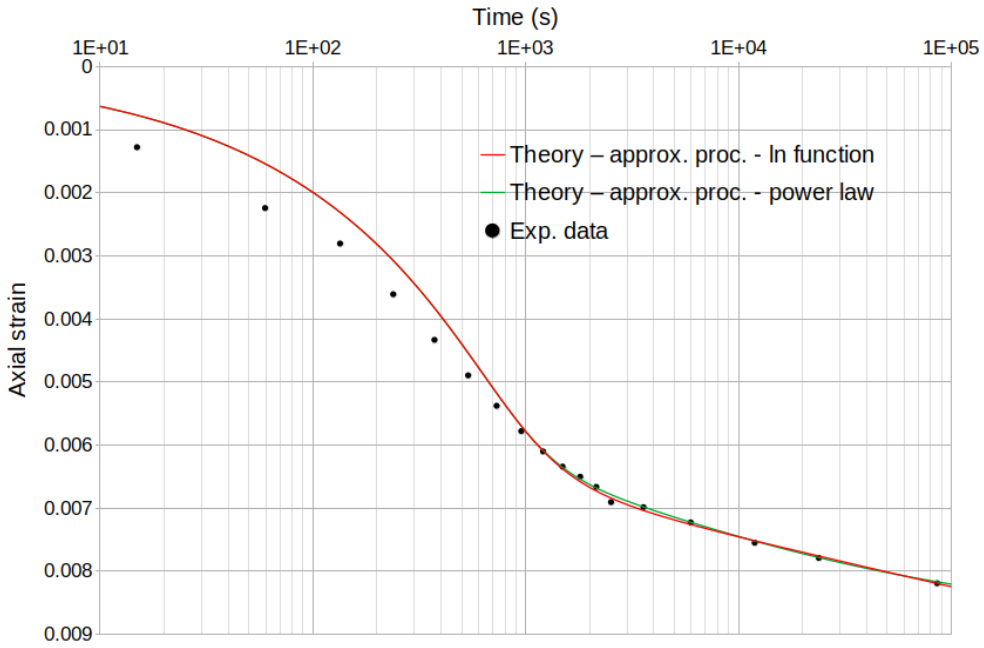

Figure 5: Experimental data and predictions.

5.3 Loading Increment №3

Parametre	Estimated value
$\Delta\sigma(kPa)$	49.0
$\bar{\epsilon}_{90}$	0.0115
$\bar{\epsilon}_{100}$	0.0128
$\bar{\epsilon}_f$	0.025
$t_{90}(s)$	870
$E_p(kPa)$	3,837
$E_s(kPa)$	4,012
$c_v(\frac{m^2}{s})$	2.36×10^{-7}
$k(m/s)$	6.04×10^{-10}

Table 3: Summary table

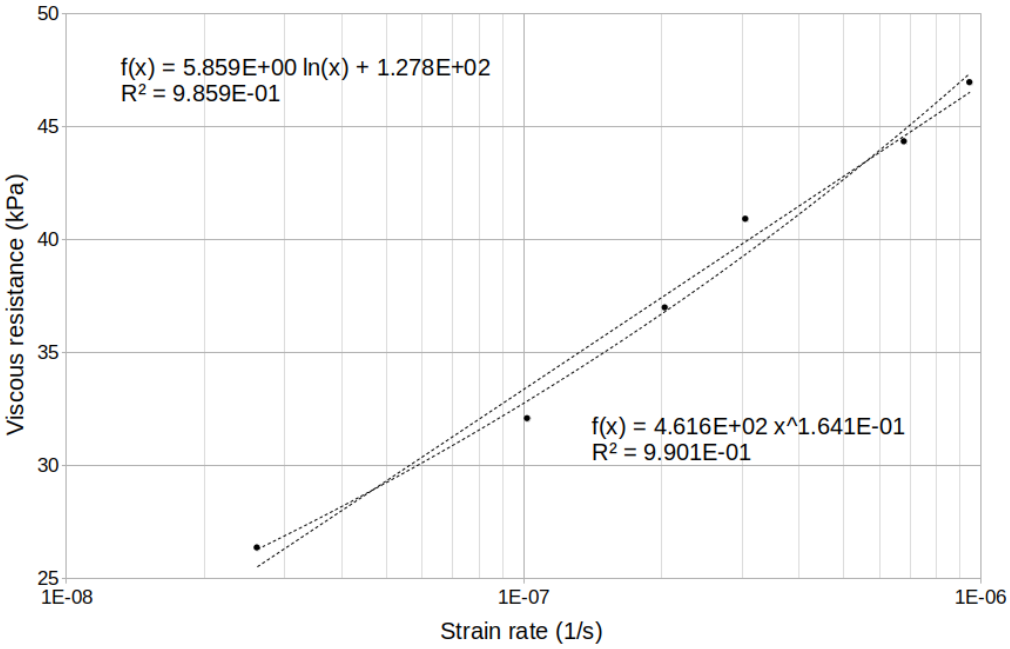

Figure 6: Estimated viscous functions.

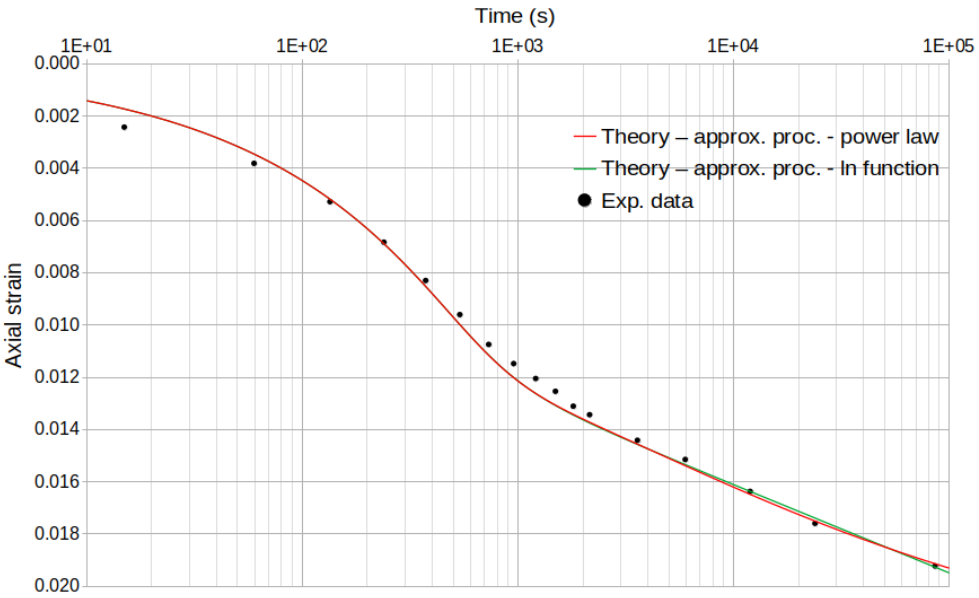

Figure 7: Experimental data and predictions.

5.4 Loading Increment №4

Parametre	Estimated value
$\Delta\sigma(kPa)$	98.1
$\bar{\epsilon}_{90}$	0.058
$\bar{\epsilon}_{100}$	0.064
$\bar{\epsilon}_f$	0.10
$t_{90}(s)$	4900
$E_p(kPa)$	1,522
$E_s(kPa)$	2,758
$c_v(\frac{m^2}{s})$	3.80×10^{-8}
$k(m/s)$	2.45×10^{-10}

Table 4: Summary table

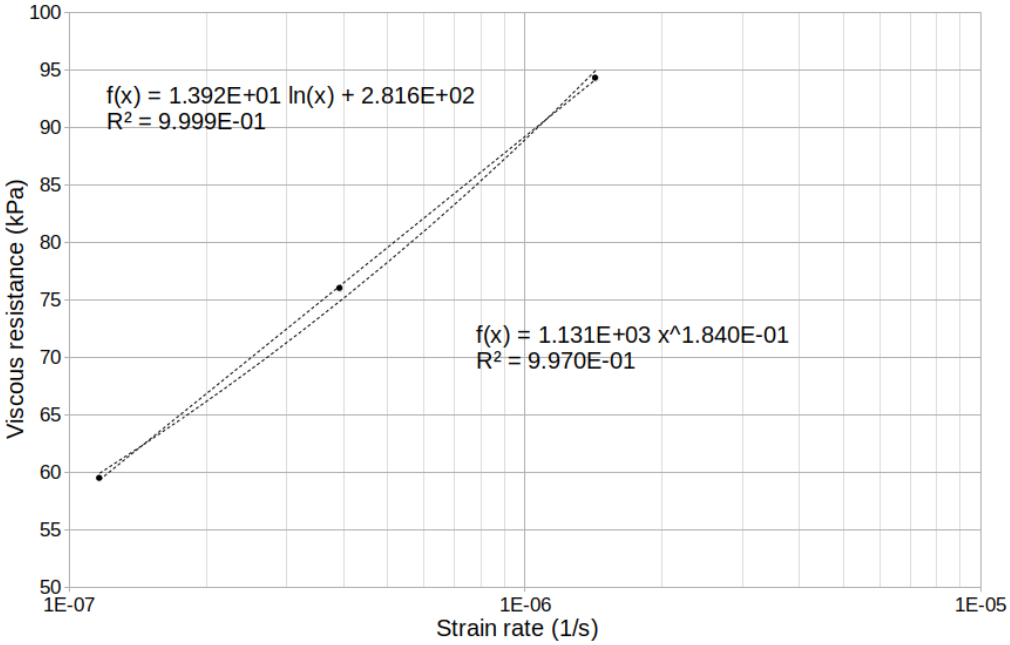

Figure 8: Estimated viscous functions.

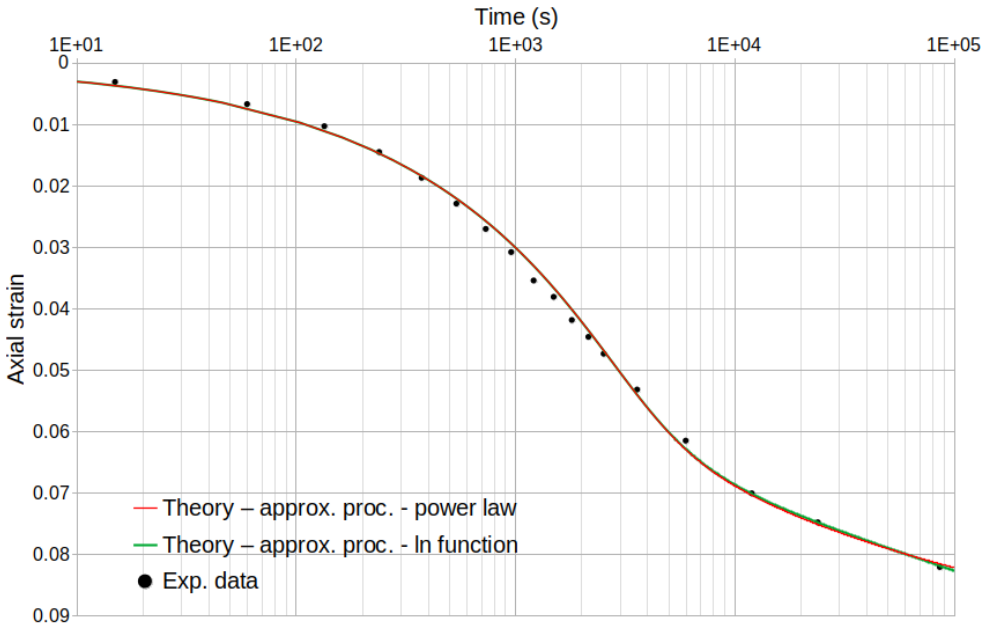

Figure 9: Experimental data and predictions.

5.5 Loading Increment №5

Parametre	Estimated value
$\Delta\sigma(kPa)$	196.1
$\bar{\epsilon}_{90}$	0.057
$\bar{\epsilon}_{100}$	0.063
$\bar{\epsilon}_f$	0.08
$t_{90}(s)$	3,540
$E_p(kPa)$	3,097
$E_s(kPa)$	11,768
$c_v(\frac{m^2}{s})$	5.31×10^{-8}
$k(m/s)$	1.68×10^{-10}

Table 5: Summary table

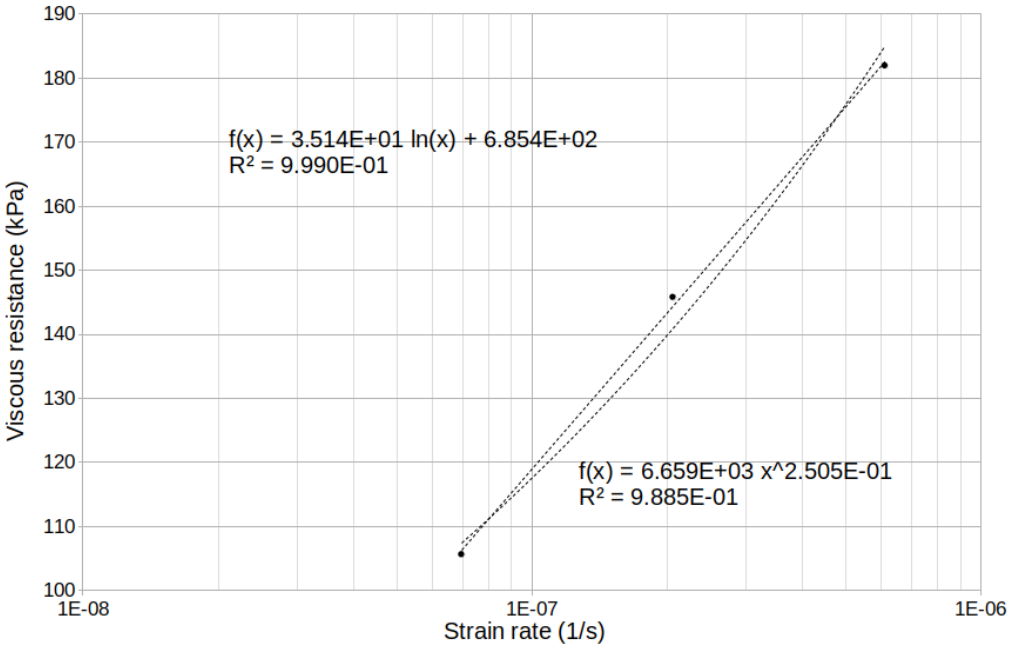

Figure 10: Estimated viscous functions.

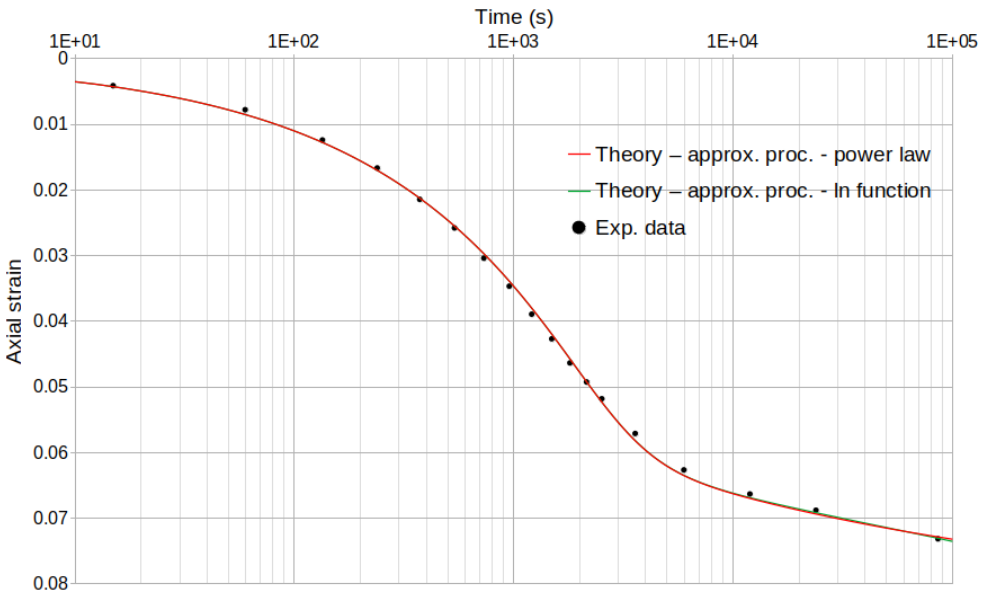

Figure 11: Experimental data and predictions.

5.6 Loading Increment №6

Parametre	Estimated value
$\Delta\sigma(kPa)$	392.3
$\bar{\epsilon}_{90}$	0.045
$\bar{\epsilon}_{100}$	0.05
$\bar{\epsilon}_f$	0.07
$t_{90}(s)$	2,025
$E_p(kPa)$	7,846
$E_s(kPa)$	19,614
$c_v(\frac{m^2}{s})$	8.09×10^{-8}
$k(m/s)$	1.01×10^{-10}

Table 6: Summary table

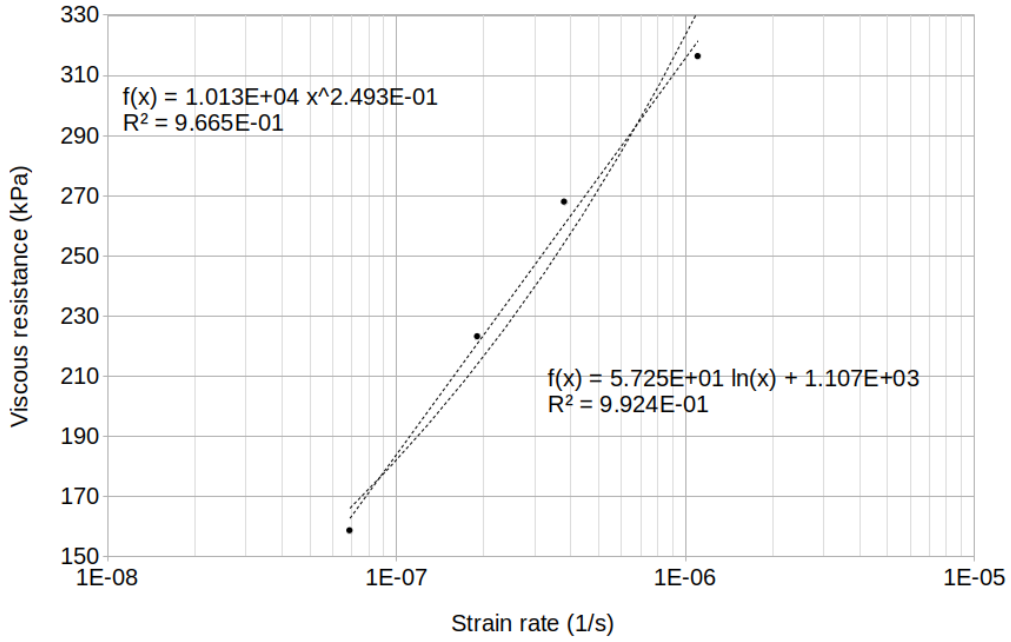

Figure 12: Estimated viscous functions.

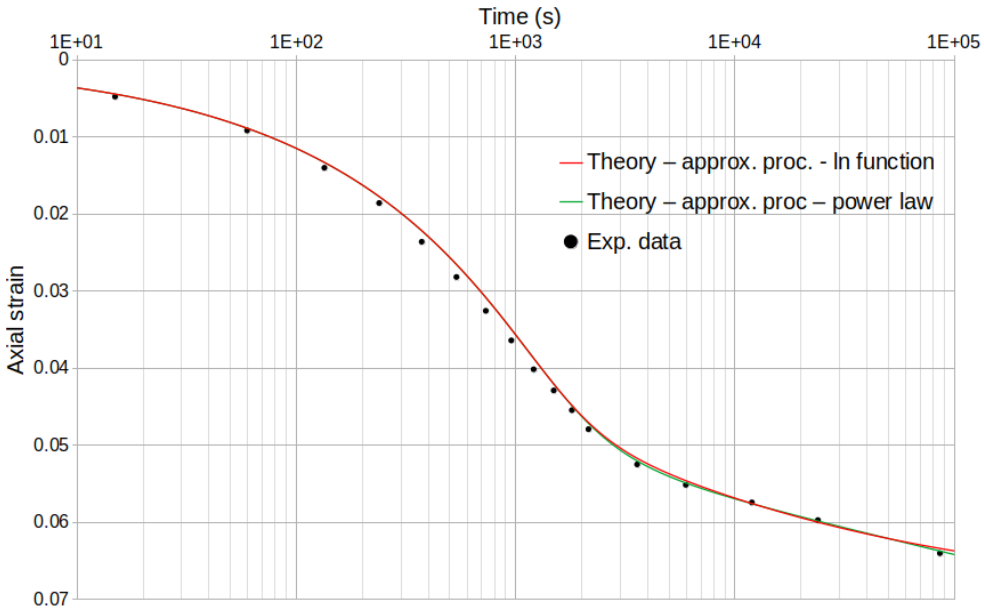

Figure 13: Experimental data and predictions.

5.7 Loading Increment №7

Parametre	Estimated value
$\Delta\sigma(kPa)$	784.6
$\bar{\epsilon}_{90}$	0.044
$\bar{\epsilon}_{100}$	0.049
$\bar{\epsilon}_f$	0.07
$t_{90}(s)$	1,296
$E_p(kPa)$	16,048
$E_s(kPa)$	37,163
$c_v(\frac{m^2}{s})$	1.11×10^{-7}
$k(m/s)$	6.81×10^{-11}

Table 7: Summary table

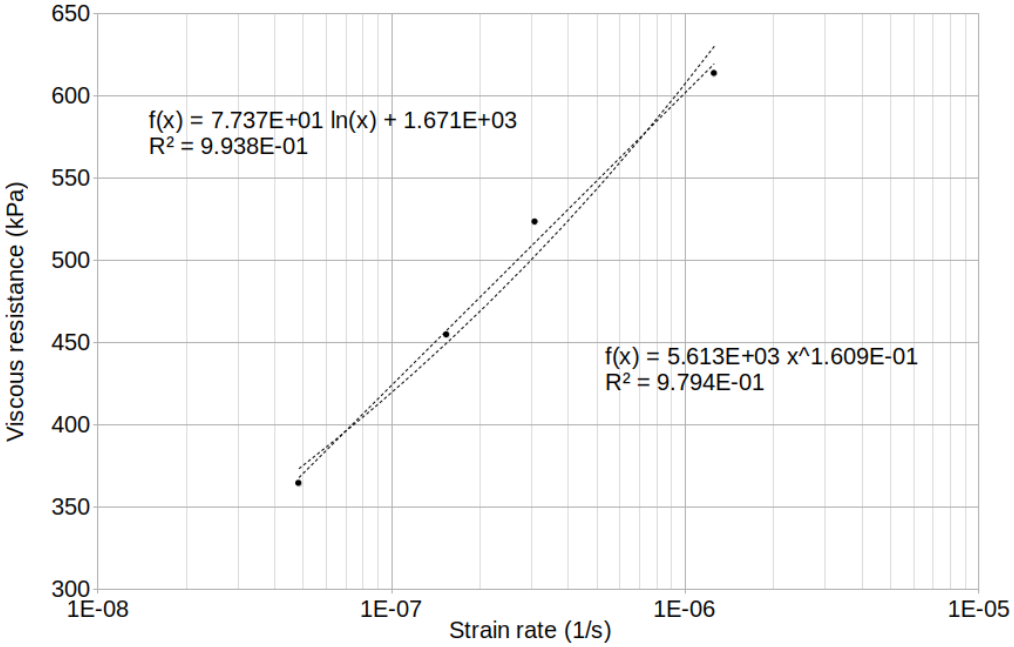

Figure 14: Estimated viscous functions.

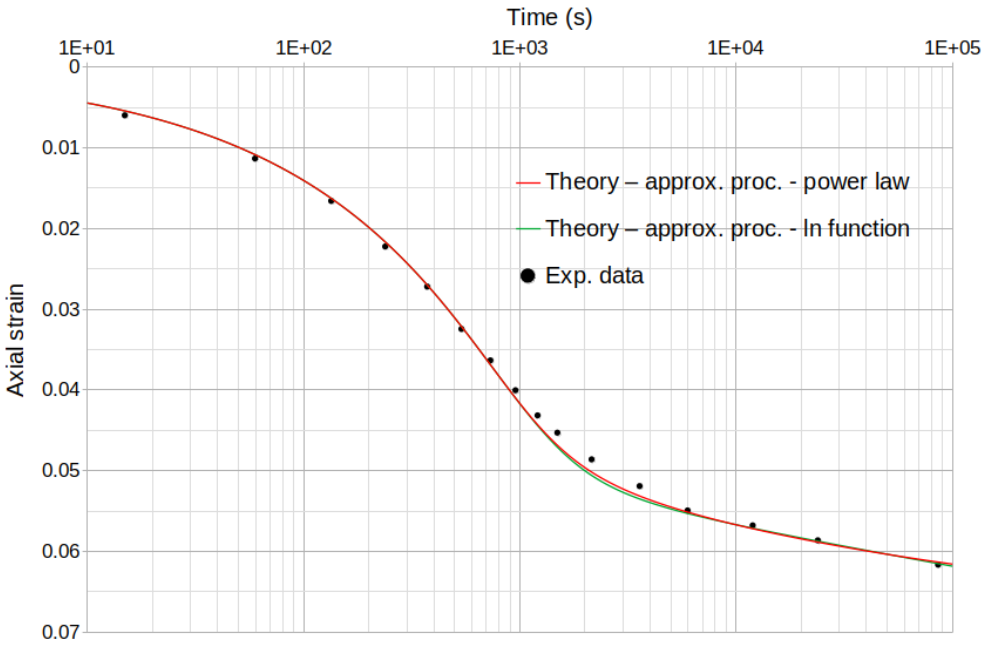

Figure 15: Experimental data and predictions.

6 Comparison with the Tests from Carvalho (1997)

The predictions presented below for the tests from Carvalho (1997) were obtained after making a slight modification regarding the assessment and modelling of the viscous function of the soil tested. Without this modification, the initial predictions showed good agreement only to the point where the test curves start to dip during secondary compression. For the moment it is sufficient to add that, for this soil, the viscosity function could not be expressed by a single function such as a power law or a logarithmic function. That said, it was found that by breaking the viscous function into two parts, each represented by a power law or a logarithmic function, it was possible to make the predictions shown below. The threshold at which the change in the viscous function occurs is noted in the tables. This important point will be detailed in the discussion section of the paper. As it was done for the tests from Taylor (1948), a summary table, a plot with the estimated viscous resistance and a second plot with the experimental results and prediction are provided for each test. Finally, the data points used herein come from the tabulated values contained in Appendix D.2 from Carvalho (1997).

6.1 Long Term Duration Test №1

Parametre	Estimated value
$\Delta\sigma(kPa)$	400
$\bar{\epsilon}_{90}$	0.089
$\bar{\epsilon}_{100}$	0.0989
$\bar{\epsilon}_f$	0.141
$t_{90}(s)$	961
$E_p(kPa)$	4,045
$E_s(kPa)$	9,567
$c_v(\frac{m^2}{s})$	5.39×10^{-8}
$k(m/s)$	1.31×10^{-10}
Strain rate threshold s^{-1}	1×10^{-9}

Table 8: Summary table

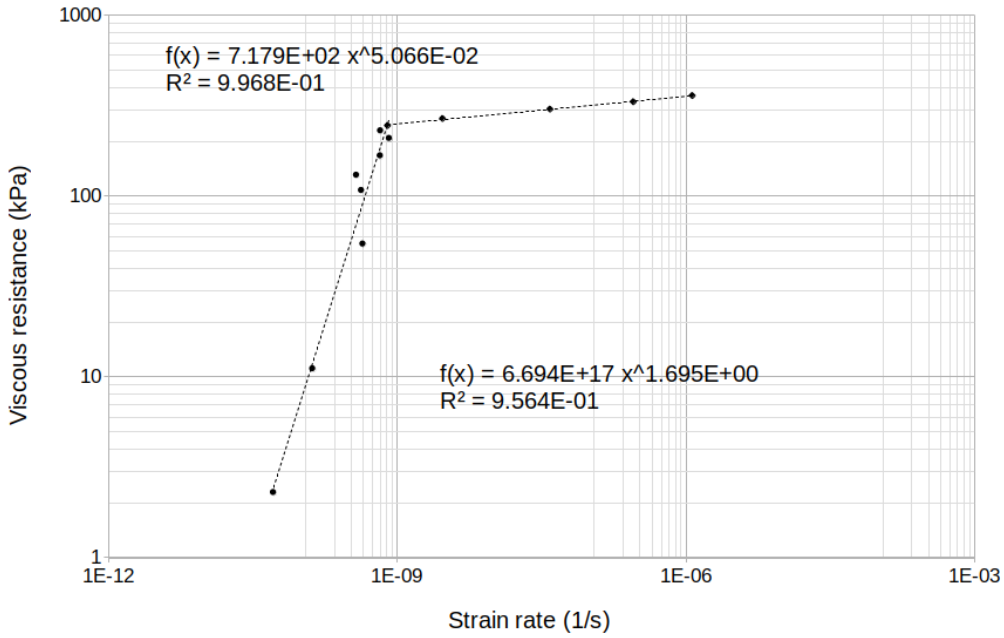

Figure 16: Estimated viscous functions.

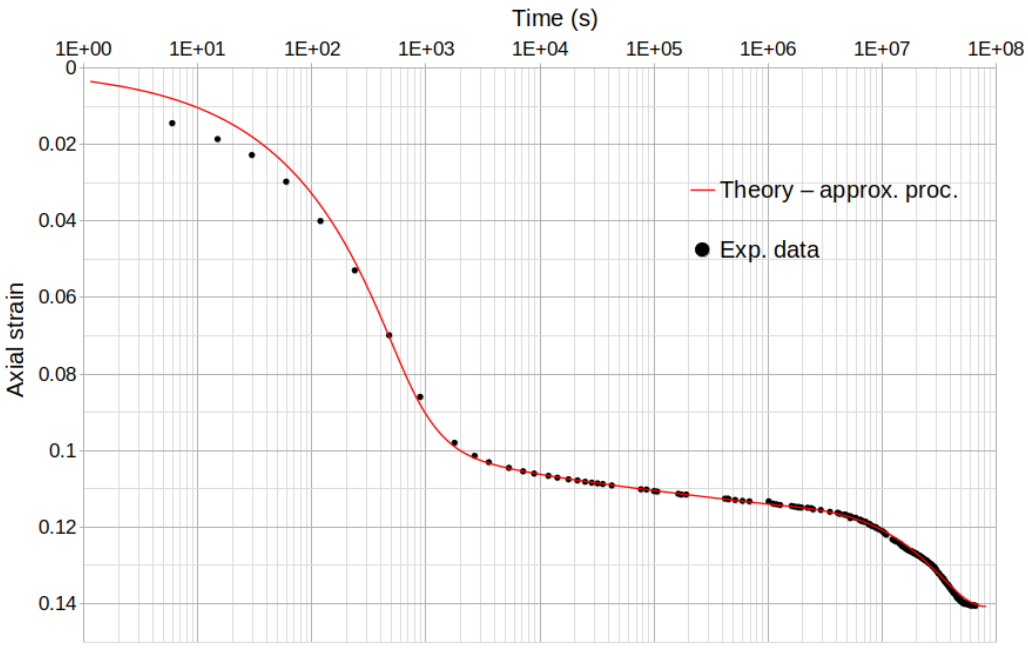

Figure 17: Experimental data and predictions.

6.2 Long Term Duration Test №2

Parametre	Estimated value
$\Delta\sigma(kPa)$	200
$\bar{\epsilon}_{90}$	0.05
$\bar{\epsilon}_{100}$	0.056
$\bar{\epsilon}_f$	0.0939
$t_{90}(s)$	961
$E_p(kPa)$	3,600
$E_s(kPa)$	5,214
$c_v(\frac{m^2}{s})$	5.83×10^{-8}
$k(m/s)$	1.59×10^{-10}
Strain rate threshold s^{-1}	1×10^{-9}

Table 9: Summary table

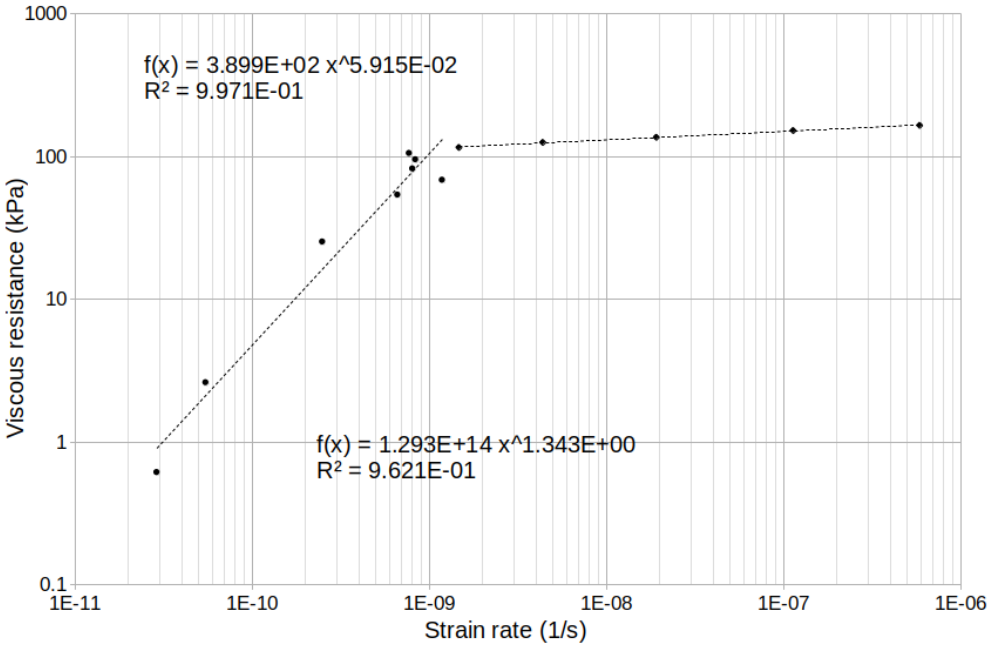

Figure 18: Estimated viscous functions.

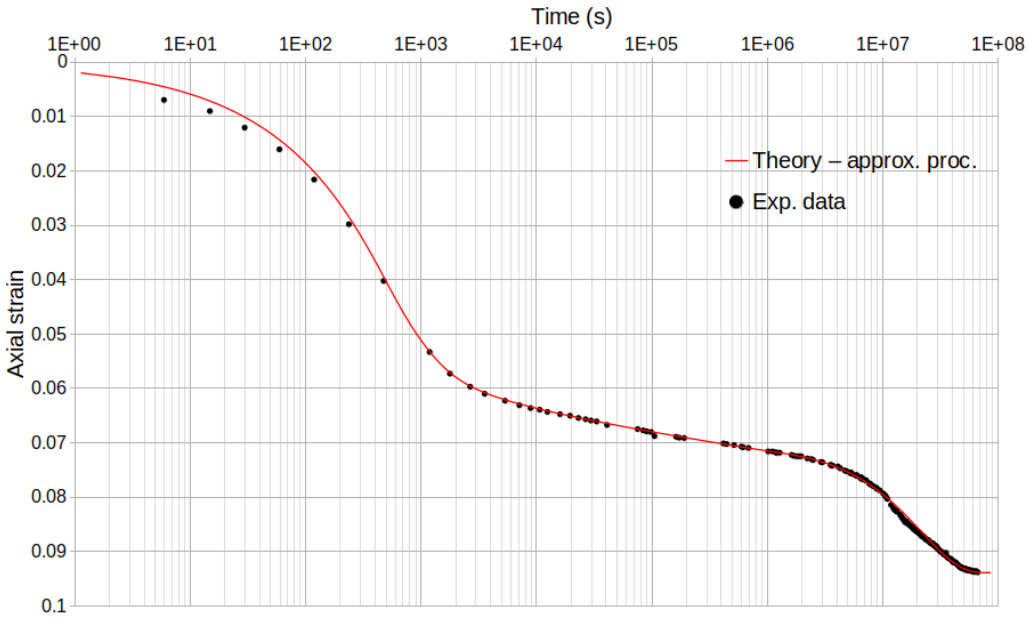

Figure 19: Experimental data and predictions.

6.3 Long Term Duration Test №3

Parametre	Estimated value
$\Delta\sigma(kPa)$	400
$\bar{\epsilon}_{90}$	0.045
$\bar{\epsilon}_{100}$	0.05
$\bar{\epsilon}_f$	0.09
$t_{90}(s)$	1,369
$E_p(kPa)$	8,000
$E_s(kPa)$	9,963
$c_v(\frac{m^2}{s})$	2.85×10^{-8}
$k(m/s)$	3.5×10^{-11}
Strain rate threshold s^{-1}	1×10^{-9}

Table 10: Summary table

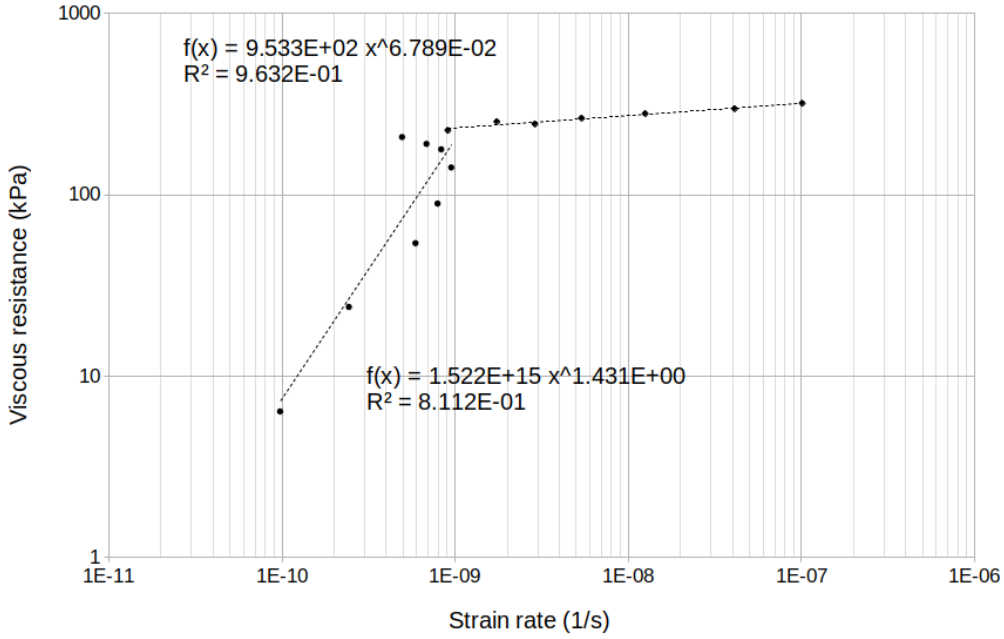

Figure 20: Estimated viscous functions.

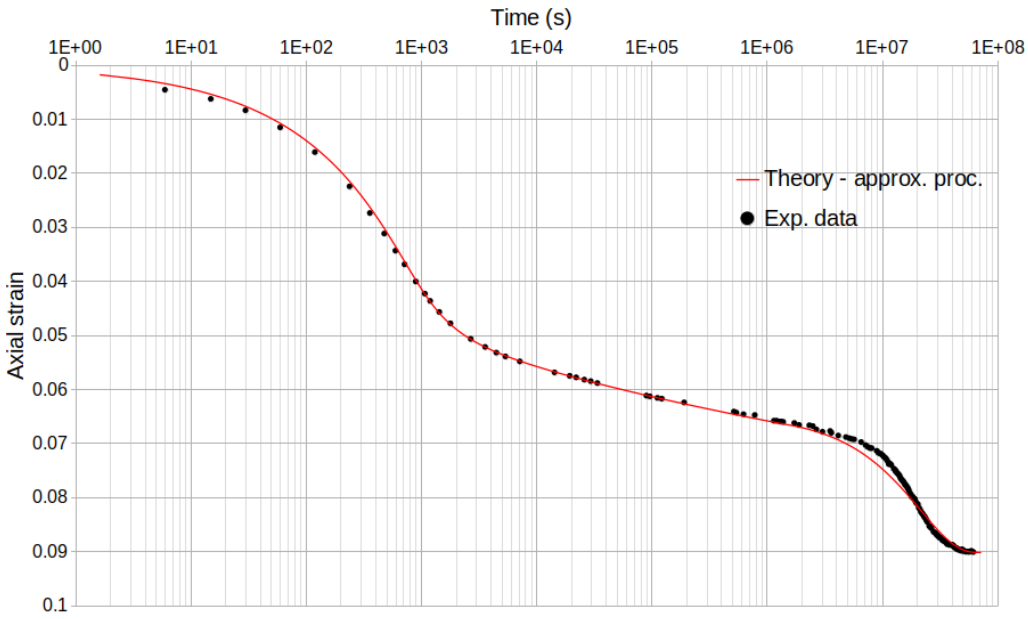

Figure 21: Experimental data and predictions.

7 Discussion

As can be seen in all tests, there is a very good agreement both qualitatively and quantitatively between predictions using the approximate procedure and experimental results. That said, specific points related to this comparison and to the numerical procedures are addressed below.

7.1 Numerical Schemes

In relation to numerical schemes, it is worth noting that all the predictions presented followed the approximate procedure described in Section 3.1 with a time-step of $\Delta T_v = 0.001$. This time interval was deemed satisfactory after comparing results with different time-steps. This can be seen in Figure 22 for the third load increment of Taylor's test, where predictions with two different time intervals were made.

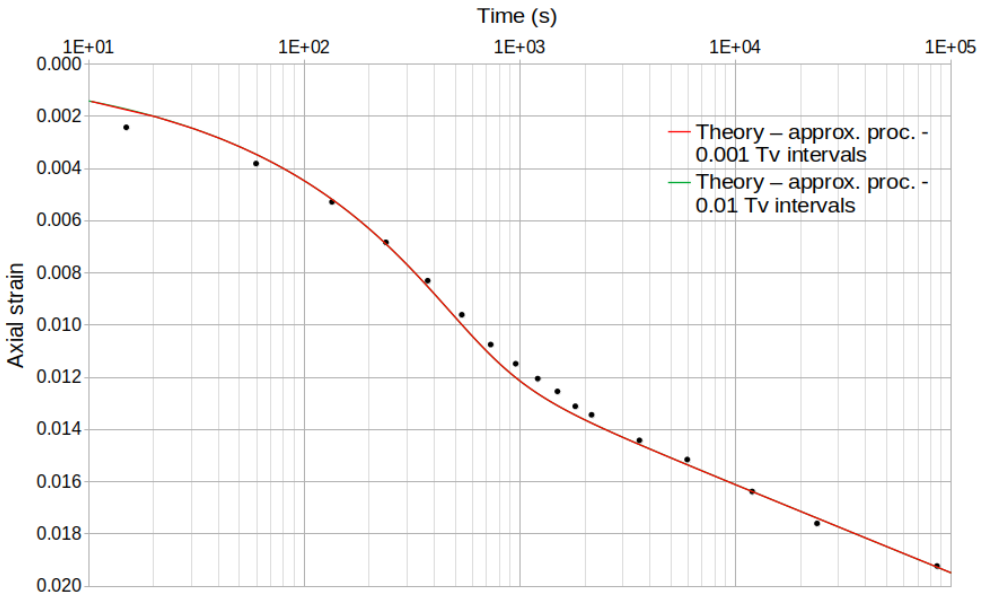

Figure 22: Comparison between two predictions using the approximate procedure for different time steps.

As can be seen above, no significant difference exists between the curves with $\Delta T_v = 0.001$ and $\Delta T_v = 0.01$. In addition, both predictions are close to the experimental data.

Figure 23 below shows a comparison for the third load increment of the

test from Taylor (1948) using the finite differences scheme and the approximate procedure.

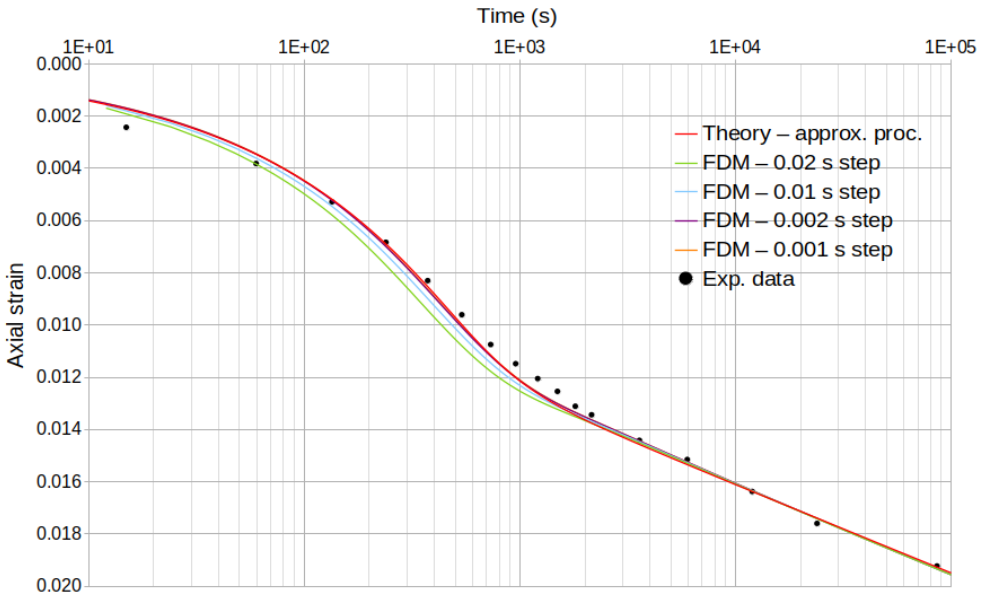

Figure 23: Comparison between the approximate procedure and the finite differences scheme for different time steps.

From Figure 23 it is clear that the adoption of smaller time-steps when using the finite differences scheme converges to a curve that is very close to the curve obtained using the approximate procedure.

The agreement between the approximate procedure and the finite differences scheme can be understood by comparing the magnitudes of the strain rates from primary consolidation and from secondary compression and observing at the same time the evolution of excess pore-pressures during the test. This will be done again for the third loading increment from Taylor's test. Figure 24 shows a plot of the ratio between the average strain rate from secondary compression and the average strain rate (primary and secondary included) of the test over time.

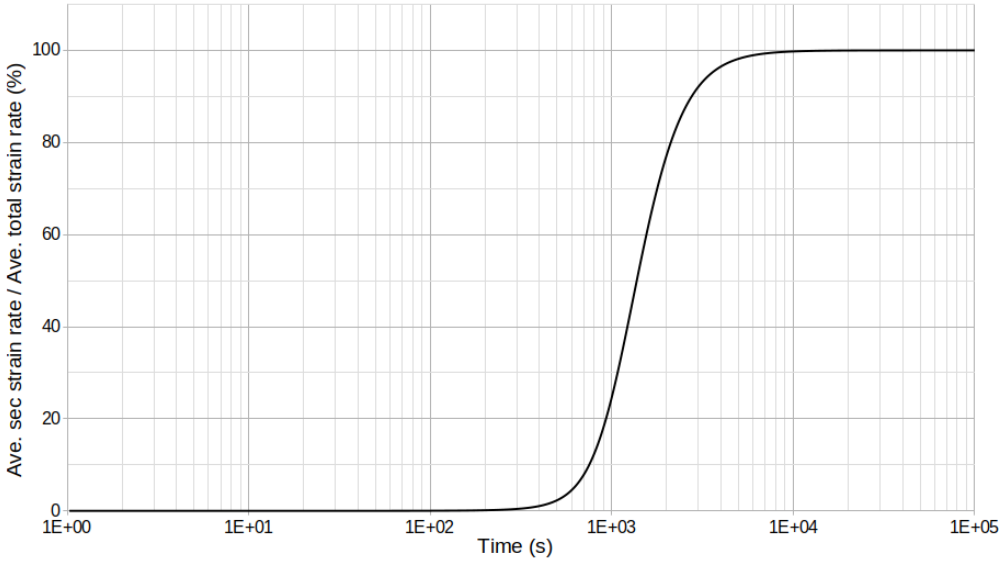

Figure 24: Ratio between the strain rate from secondary compression and total strain rate for loading increment №3 (prediction).

From Figure 24 it can be seen that the average strain rate from secondary compression is less than 10% of the average total strain rate of the test from the beginning of the test up to $750s$. That is, the contribution from secondary compression to the strain rate of the test is very small for a great part of primary consolidation. Having in mind Equation 5 - $\frac{k}{\gamma_w} \cdot \frac{\partial^2 \sigma'}{\partial z^2} = \frac{1}{E_p} \cdot \frac{\partial \sigma'}{\partial t} + \frac{\partial \epsilon_s}{\partial t}$ - for very small strain rates from secondary compression, the process is essentially in accordance to Terzaghi's theory. That is, Equation 5 becomes $\frac{k}{\gamma_w} \cdot \frac{\partial^2 \sigma'}{\partial z^2} = \frac{1}{E_p} \cdot \frac{\partial \sigma'}{\partial t}$.

On the other hand, as can be seen in Figure 25, after about $1,000s$, the predicted excess pore-pressure is about 10% of the total stress increment for this test stage, which is $\Delta\sigma = 49kPa$. That is, after about $1000s$, the resistance to compression from the transient flow is very small and the process is governed by the structural viscous resistance to compression represented by the Kelvin-Voigt body.

All in all, it seems clear that the overlapping of these two processes - transient flow and structural viscous resistance to compression - is most significant in a relatively narrow range in time that spans from the midpoint to the end of primary consolidation.

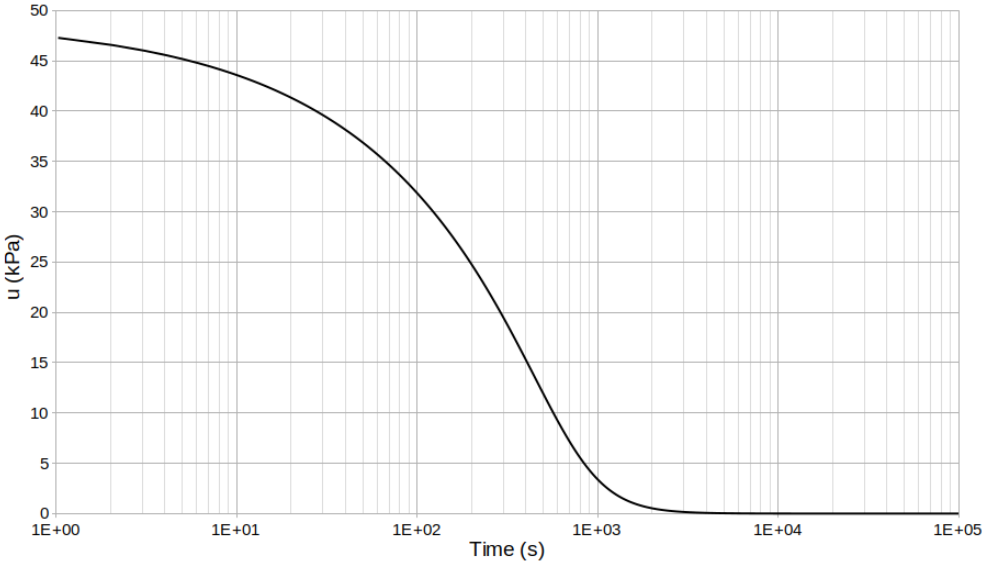

Figure 25: Estimated excess pore-pressure for loading increment №3.

7.2 Rheological Models and the Generation of Excess Pore-pressure

As it happens with the original theory from Gibson and Lo (1961), the excess pore-pressure at $t = 0^+$ in the new theory is equal to total stress increment ($u = \Delta\sigma$) as it is also, of course, in Terzaghi's theory. This is an important point when it comes to discussing the many theories put forward for explaining the secondary compression of soils.

For the line of theories which can be characterized by Taylor's "Theory B" and by Barden's theory (Barden 1965) [10], the action of the structural viscous resistance to compression is such that the excess pore-pressure at $t = 0^+$ is always less than the total stress increment, $\Delta\sigma$. This is in contraposition to the theory by Gibson and Lo (1961) and the new theory presented in this paper.

The validity of these lines of theories can then be tested based on the experimental evidence regarding the excess pore-pressure at the beginning of the tests. However, the measuring of the excess pore-pressure at $t = 0^+$ is not straightforward because any pore-pressure measuring device has a basic time-lag response. That said, a recent paper by Chow et al (2020) [11] clearly shows that the excess pore-pressure at $t = 0^+$ is indeed equal to the total stress increment. Therefore, it is concluded that the present theory is also in

agreement with the experimental evidence regarding the excess pore-pressure generation at the beginning of the test.

As can be seen in Figure 26, it appears also that the approximate procedure is able to produce good results regarding the excess pore-pressure when compared to the finite differences scheme. More importantly, the transition from primary consolidation to secondary compression is gradual in terms of excess pore-pressures.

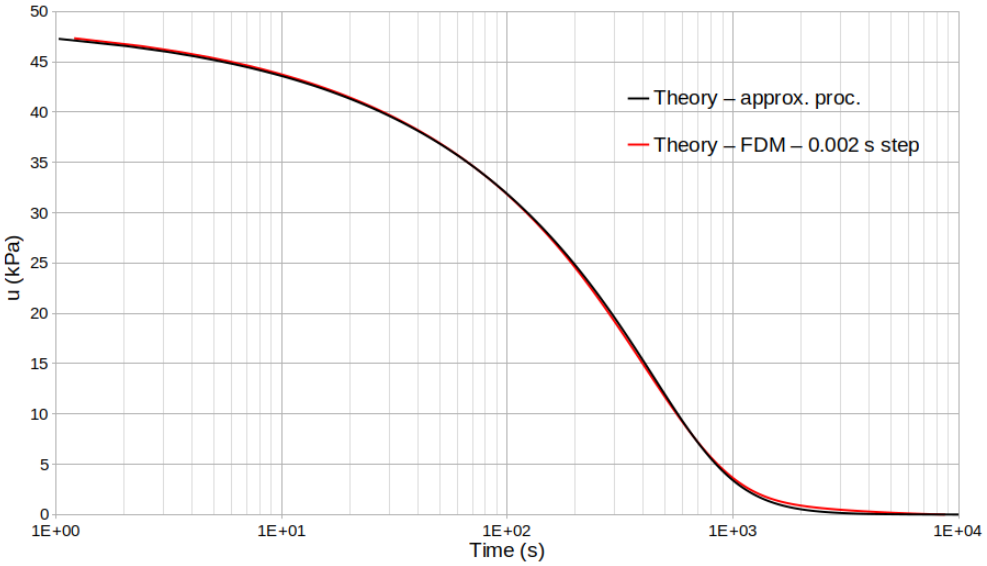

Figure 26: Generated excess pore-pressure from the approximate procedure and from the finite differences scheme.

7.3 The Tests from Taylor (1948)

As mentioned in the beginning of this section, overall, the predictions are in very good agreement with the experimental results. That said, some important points regarding the tests reported by Taylor (1948) and the predictions made for these tests require additional discussions.

One important point is related to the final strain $\bar{\epsilon}_f$. As the loading increments were all of about a day, no final strain was reached when the stages were interrupted. As such, the final strains presented in the summary tables for these tests are therefore only guesses. That said, adoption of other final strains of the same order of magnitude do not seem to alter much the predictions. As an exercise, Figure 27 shows the comparison between

the original prediction made with $\epsilon_f = 0.025$ and a new prediction with $\epsilon_f = 0.05$. As can be seen the predictions are indeed very similar.

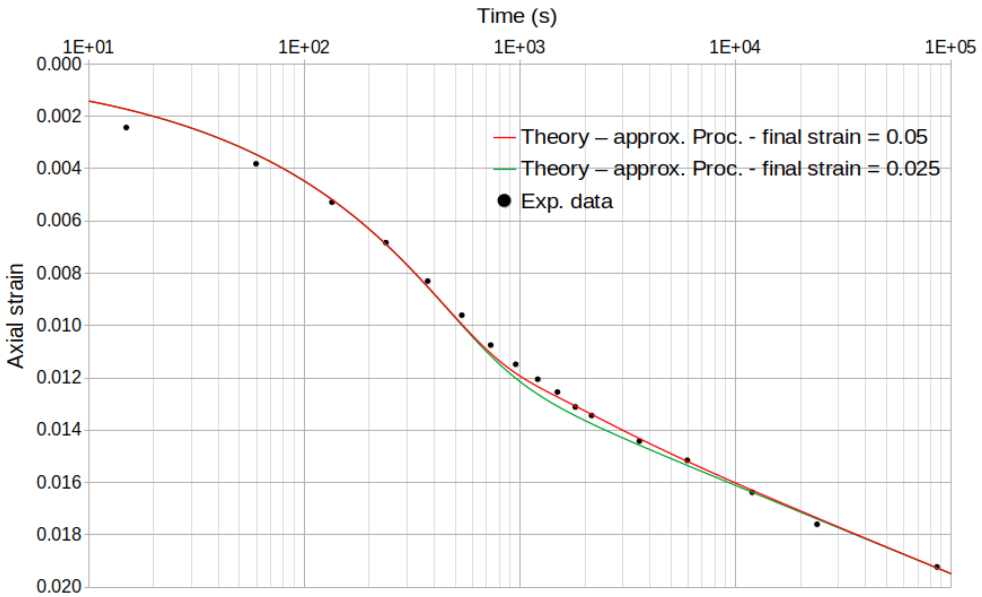

Figure 27: Comparison of the influence of the final strain on the predictions using the approximate procedure.

Another important point is the discrepancy between predictions and test results regarding the initial part of the curves as observed in Loading Increments 1 to 3. This difference is however not specific of the present theory since in the beginning of the process the transient flow and deformation from Terzaghi's theory dominates the overall response of the soil. To show that this is indeed the case, Figure 28 shows for Loading Increment number 3, in addition to the experimental results and the prediction from the new theory, the axial strain vs. time curve from Terzaghi's theory. As can be seen, Terzaghi's curve is almost entirely coincident with the curve from the new theory from the beginning up to an axial strain of about 1.1%.

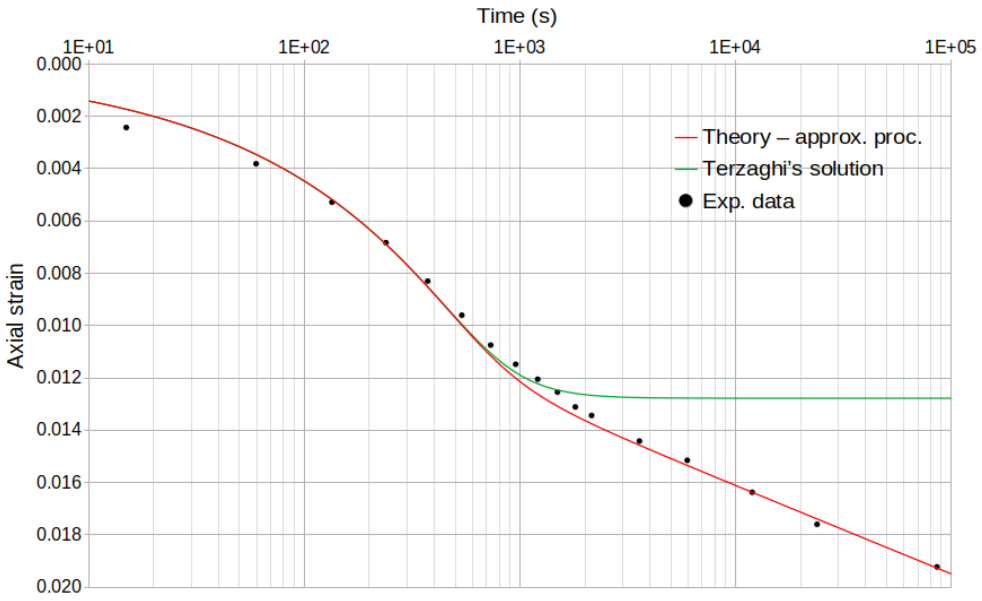

Figure 28: Comparison between the approximate procedure and Terzaghi's solution.

The third point worth discussing is the shape of the secondary compression tail of the curves. As can be seen most notably on Loading Increment №3, the later portions of the curves for the experimental data and for the new theory (when a logarithmic viscous function is used), are straight lines in the axial strain vs. time (log scale) coordinate system. This has been observed since at least the works of Gray (1936) [12] and Buisman (1936) [13]. From the point of view of the physics of the process, as pointed out by other researchers, the adoption of any logarithmic function of time for describing the evolution of secondary compression should be viewed and used with caution since the process must end one day. In the words of Lo (1961) [14], "In fact, the validity of the logarithmic law must be bounded, otherwise it would lead to the absurdity that the sample could vanish in a laterally-confined condition".

As it will be seen in the discussion section regarding the long-term tests from Carvalho (1997), the validity of logarithmic functions is indeed limited. That said, the use of such a function might be justified in the absence of long-term experimental data that shows otherwise. In addition, as used in the present theory, the logarithmic function has the strain rate as argument and it is bounded by the value of the viscous resistance to compression, which cannot fall below zero. The implication of such a function is that

secondary compression will have an end for a finite time t when the strain rate during secondary compression drops below the value of $\frac{e^{\frac{-B}{A}}}{C}$, as mentioned before. Although this is, of course, a shortcoming of the new theory when a logarithmic viscous function of the strain rate is used, it is still better than an unbounded logarithmic functions of the time t. It is also worth noting that the straight secondary tail (in the axial strain vs. time in log scale space) is a theoretical consequence of adopting a logarithmic viscous function as was shown in Alexandre (2017). Although both the power law and the logarithmic viscous function resulted in good predictions for all the loading increments for the test from Taylor (1948) for the range in time that include up to the last experimental point, beyond these last points the predictions diverge significantly as can be seen in Figure 29 for Loading increment №4.

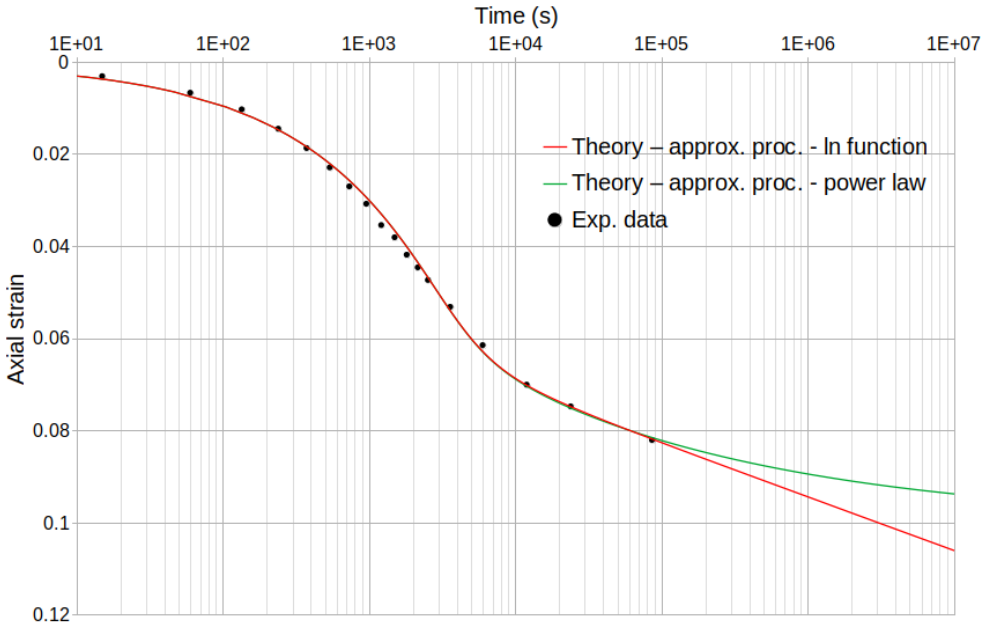

Figure 29: Divergence between predictions made with the power law viscous function and the logarithmic viscous function for Loading Increment №4.

7.4 The Tests from Carvalho (1997)

The three tests carried out by Carvalho (1997) on a soil fabricated in a laboratory comprised of 90% Caulin and 10% Bentonite lasted for about 2 years when secondary compression ended. The difference between these tests and short-term conventional tests that last about a day each loading increment is apparent. While the secondary compression tails of conventional

tests resemble straight lines in an axial strain vs. time (log scale) plot, in the long-term tests from Carvalho (1997) the tail is a straight line only to a certain point in time when the curves dip down before reaching the end of the test. Although it could be argued that these results are perhaps only characteristic of a soil fabricated in the laboratory, similar behaviour has been reported by Bishop and Lovenbury (1969) [15] and Yilmaz and Saglamer (2001) [16] for natural clays.

For these three tests, predictions were made in the same way as before for the tests from Taylor (1948). The results of the initial predictions for test №1 using a single power law or a single logarithmic function are shown in Figure 30.

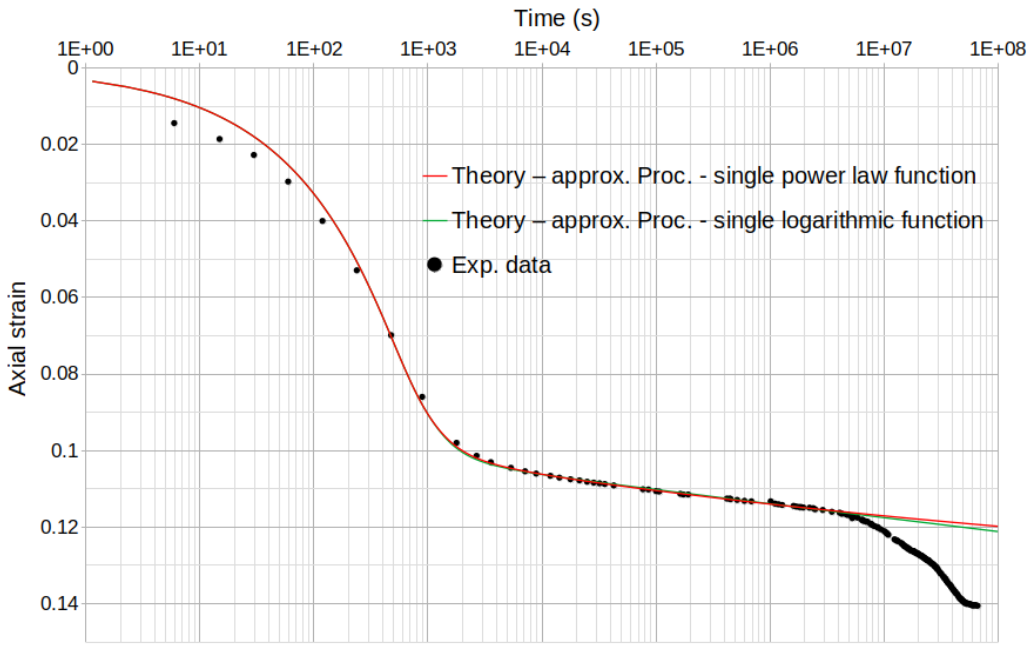

Figure 30: Initial predictions for test №1 from Carvalho (1997).

The difference between these long-term tests and the conventional ones can be explained in terms of the behaviour of their respective viscous functions. While in conventional tests, the viscous functions are "well behaved" and can be described by a single mathematical function, the same cannot be said of the long-term tests. In the latter, the relationship between viscous resistance and strain rates is complex. In all the three tests from Carvalho (1997) the initial part of the viscous function can be represented by either a single power law or a single logarithmic function only for strain rates above

a strain rate of $1 \times 10^{-9} s^{-1}$. At this strain rate, the viscous resistance to compression drops abruptly. Below this threshold, the viscous resistance to compression becomes once again "well behaved" and can be satisfactorily described by a different power law or a different logarithmic function. This abrupt drop in viscous resistance significantly increases the difficulty in representing the viscous resistance to compression as a function of the strain rate. That said, this problem can be dealt with numerically by specifying different viscous functions on each side of the strain rate threshold. This was carried out in all three tests and the results corroborate the idea that, in spite of the sharp drop in viscous resistance, the behaviour of the soil during secondary compression is still viscous in nature and therefore can be addressed in the same manner as before. The only difference however is that, during secondary compression, when the strain rate reaches the threshold then a different viscous resistance function must be used. This approach is different from the one used by Lo (1961). Lo (1961) added a second linear Kelvin-Voigt body that is activated when a certain axial strain is reached.

As a side note, a remarkable feature of this fabricated soil is that its viscous resistance to compression can be normalized in relation to the total stress increment, $\frac{\sigma'_{visc}}{\Delta\sigma}$. This can be seen in Figure 31 as well as the strain rate threshold of $1 \times 10^{-9} s^{-1}$.

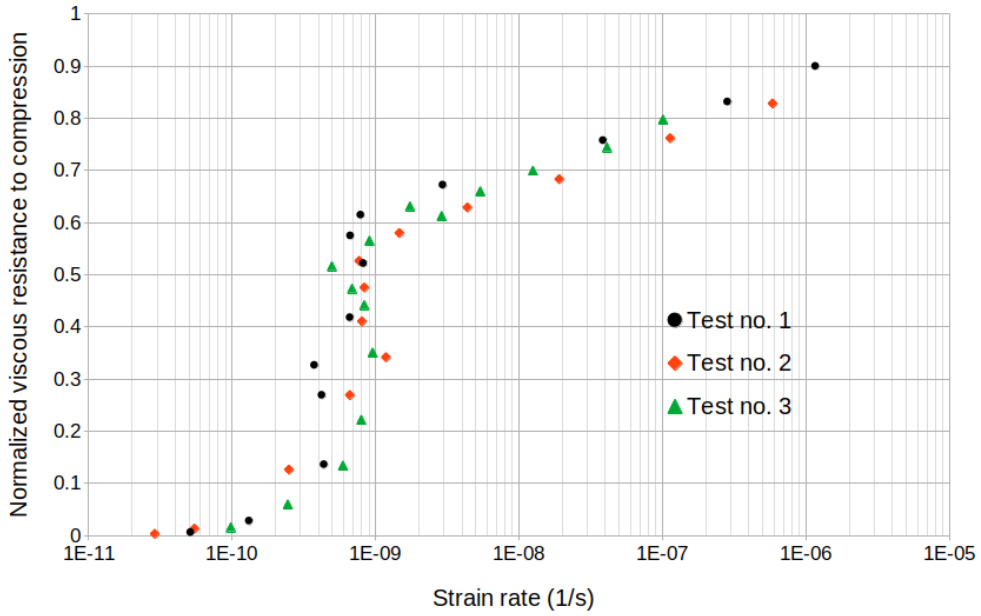

Figure 31: Normalized viscous resistance curves for the three tests from Carvalho(1997).

Finally, it is worth discussing the abrupt change in viscous behaviour observed in the three tests from Carvalho (1997). Figure 32 below shows the evolution of the strain rate over time in a log-log scale, associated with abrupt change in viscous resistance is an increase in strain rate.

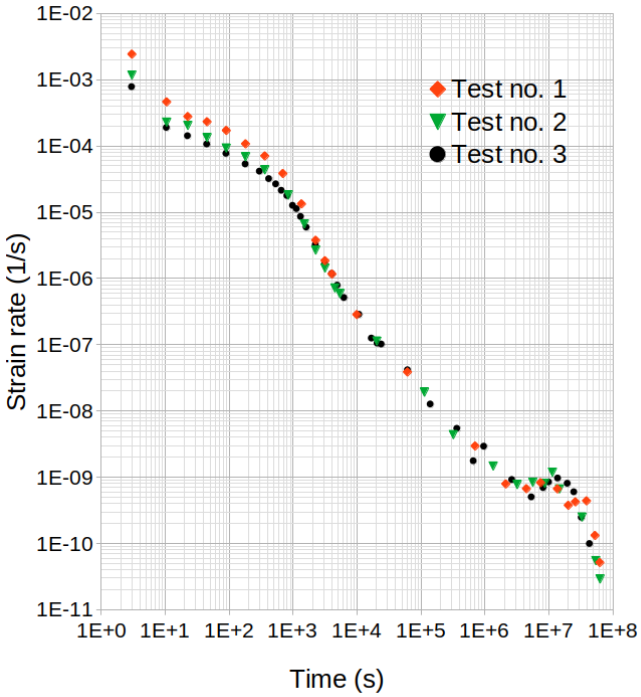

Figure 32: Strain rate vs. time curves for the tests from Carvalho (1997).

As can be seen in Figure 32 the strain rate continuously decreases until a minimum is reached. Once this minimum is reached, the strain rate increases slightly, passes thru a peak and then decreases. This unexpected behaviour has been observed before by Bishop and Lovenbury (1969) [15] and, in accordance to them, this is not related to problems in the equipment or experimental procedures. This surprising behaviour deserves more attention and research since this is not what one would expect regarding the behaviour of common rheological models such as a Kelvin-Voigt body, where the strain rate continuously decreases over time. Dispite this problem, the predictions made with new theory agree very well regarding the evolution of strain rate over time as can be seen in Figure 33 below for test №2.

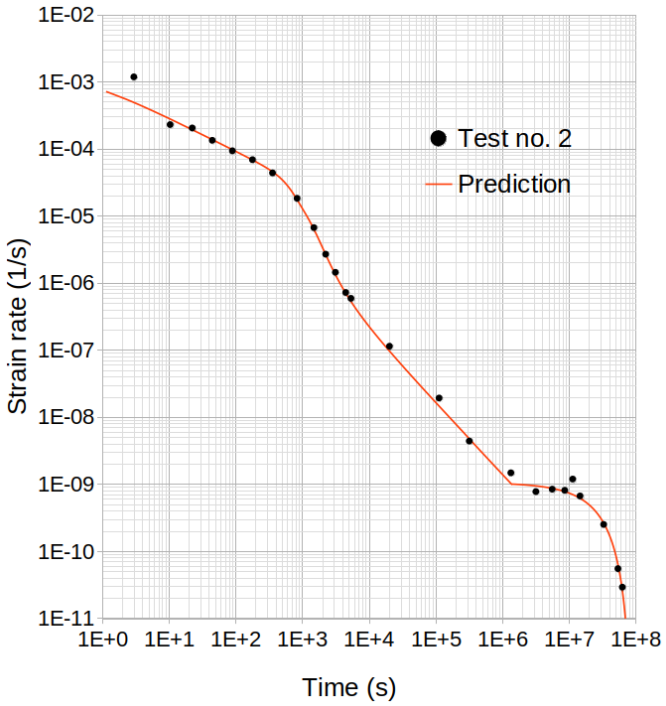

Figure 33: Strain rate vs. time curves for test №2 from Carvalho (1997).

7.5 Hypothesis A vs. Hypothesis B

An active point of discussion regarding the modelling of secondary compression is about the magnitude of the strain at the end of primary consolidation when laboratory test results are extrapolated to field conditions. This is known as the "Hypothesis A vs. Hypothesis B" discussion as framed by Ladd (1977) [17]. In light of this discussion and without entering into the details or merits of each hypothesis, it is worth noting that the new theory can be categorized as complying with Hypothesis B. As an illustration, Figure 34 shows the prediction for Loading increment №4 for the power law function used in Figure 9 when scaled to a drainage distance of 1 m.

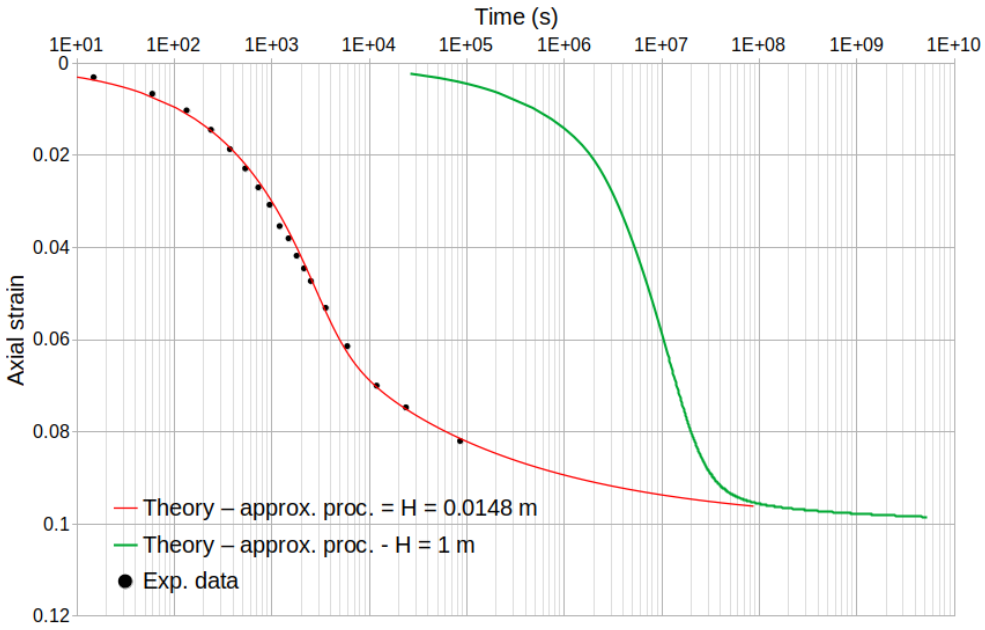

Figure 34: Example of scaling effect in accordance to the new theory using the approximate procedure.

This result can be interpreted in the light of the structural resistance to compression represented by the Kelvin-Voigt body when the drainage distance of the clay layer is changed. In accordance with the new theory (as it is also the case with the theory from Gibson and Lo, 1961), secondary compression is activated by primary consolidation which in turn depends on the drainage distance. The effect of reducing the drainage distance is speeding up primary consolidation. This, in turn, means a faster loading on the Kelvin-Voigt body. Consequently, the resistance provided by the dashpot is much more pronounced the shorter the drainage distance is. In other words, secondary compression is suppressed more in the laboratory than it is in the field. The end result is that the lumping of the contributions to total strain from primary consolidation and secondary compression yield greater strains at the "end of primary" in the field when compared to laboratory results. This conclusion is the same regardless of the viscous function used, of course.

7.6 Structural Viscous Resistance to Compression

The equations used for representing and modelling the viscous resistance to compression in all tests analyzed in this paper are summarized in Tables 11

and 12 below together with their respective correlation coefficients.

Load. inc. №	Power law	R^2	Nat. log function	R^2
1	$\bar{\sigma}_{visc} = 69.5 \cdot \frac{d\bar{\epsilon}_s}{dt}^{0.123}$	0.903	$\bar{\sigma}_{visc} = 25.4 + 0.98 \cdot \ln(1s \cdot \frac{d\bar{\epsilon}_s}{dt})$	0.938
2	$\bar{\sigma}_{visc} = 830 \cdot \frac{d\bar{\epsilon}_s}{dt}^{0.234}$	0.994	$\bar{\sigma}_{visc} = 72.7 + 3.34 \cdot \ln(1s \cdot \frac{d\bar{\epsilon}_s}{dt})$	0.982
3	$\bar{\sigma}_{visc} = 462 \cdot \frac{d\bar{\epsilon}_s}{dt}^{0.164}$	0.990	$\bar{\sigma}_{visc} = 128 + 5.86 \cdot \ln(1s \cdot \frac{d\bar{\epsilon}_s}{dt})$	0.986
4	$\bar{\sigma}_{visc} = 1,131 \cdot \frac{d\bar{\epsilon}_s}{dt}^{0.184}$	0.997	$\bar{\sigma}_{visc} = 282 + 13.9 \cdot \ln(1s \cdot \frac{d\bar{\epsilon}_s}{dt})$	0.999
5	$\bar{\sigma}_{visc} = 6,659 \cdot \frac{d\bar{\epsilon}_s}{dt}^{0.251}$	0.989	$\bar{\sigma}_{visc} = 686 + 35.1 \cdot \ln(1s \cdot \frac{d\bar{\epsilon}_s}{dt})$	0.999
6	$\bar{\sigma}_{visc} = 10,130 \cdot \frac{d\bar{\epsilon}_s}{dt}^{0.249}$	0.967	$\bar{\sigma}_{visc} = 1,107 + 57.3 \cdot \ln(1s \cdot \frac{d\bar{\epsilon}_s}{dt})$	0.992
7	$\bar{\sigma}_{visc} = 5,613 \cdot \frac{d\bar{\epsilon}_s}{dt}^{0.161}$	0.979	$\bar{\sigma}_{visc} = 1,671 + 77.4 \cdot \ln(1s \cdot \frac{d\bar{\epsilon}_s}{dt})$	0.994

Table 11: Summary of viscous functions and their respective correlation coefficients for the loading increments from Taylor (1948).

Long-term test №	1^{st} power law	R^2	2^{nd} power law	R^2
1	$\bar{\sigma}_{visc} = 718 \cdot \frac{d\bar{\epsilon}_s}{dt}^{0.051}$	0.997	$\bar{\sigma}_{visc} = 6.69 \cdot 10^{17} \cdot \frac{d\bar{\epsilon}_s}{dt}^{1.695}$	0.956
2	$\bar{\sigma}_{visc} = 390 \cdot \frac{d\bar{\epsilon}_s}{dt}^{0.059}$	0.997	$\bar{\sigma}_{visc} = 1.29 \cdot 10^{14} \cdot \frac{d\bar{\epsilon}_s}{dt}^{1.343}$	0.962
3	$\bar{\sigma}_{visc} = 953 \cdot \frac{d\bar{\epsilon}_s}{dt}^{0.068}$	0.963	$\bar{\sigma}_{visc} = 1.52 \cdot 10^{15} \cdot \frac{d\bar{\epsilon}_s}{dt}^{1.431}$	0.811

Table 12: Summary of viscous functions and their respective correlation coefficients for the loading increments from Carvalho (1997).

As can be seen in Tables 11 and 12, the great majority of the functions used for describing the viscous resistance to compression exhibited very high correlation coefficients (in general over 0.95, $R^2 \geq 0.95$). This, in turn, is indicative of the soundness of the mathematical description of these functions as well as of the theory.

8 Conclusions

Considering the comparison between what was predicted with the new theory and the experimental results from conventional and long-term tests the following can be concluded for these two soils:

- Secondary compression can be explained, modelled and predicted solely on the basis of the viscous nature of the soil;
- Power law or logarithmic functions either by themselves or combined can be used to accurately model secondary compression;
- The new theory for the modelling of secondary compression of saturated soils under vertical flow and deformation, which makes use of non-linear viscous functions such as power law or logarithmic functions, can represent very well the entire process both in qualitative and quantitative terms; and
- The approximate procedure, which in essence transforms the non-linear partial differential equation of the process into a non-linear ordinary differential equation was capable of representing it very well for all the loading increments studied in this paper.

9 Changes from Original Working Paper

The original working paper was corrected for typos and updated for including additional references as well as for the clarification of nomenclature and symbols. Among several typos were the values of the coefficient of consolidation and permeability of the tests from Carvalho (1997). The previous values were due to incorrect drainage distances from preliminary analysis of these tests. One reference - Buisman (1936) - was added.

10 Acknowledgements

The authors would like to express their sincere appreciation to Professor Emeritus John Schmertann and Professor Emeritus K. Y. Lo for their comments.

References

[1] RE Gibson and KY Lo. A theory of consolidation for soils exhibiting secondary compression. *Norwegian Geotechnical Institute, Publication*, (41), 1961.

[2] Donald W Taylor. *Fundamentals of soil mechanics*. John Wiley and Sons, 1948.

[3] S. R. L. Carvalho. *Uma Teoria de Adensamento com Compressão Secundária*. PhD thesis, COPPE/UFRJ - Instituto Alberto Luiz Coimbra de Pós-Graduação e Pesquisa em Engenharia, 1997.

[4] S Leroueil, M Kabbaj, F Tavenas, and R Bouchard. Stress–strain–strain rate relation for the compressibility of sensitive natural clays. *Géotechnique*, 35(2):159–180, 1985.

[5] I. S. M. Martins. *Fundamentos de um Modelo de Comportamento de Solos Argilosos Saturados*. PhD thesis, COPPE/UFRJ - Instituto Alberto Luiz Coimbra de Pós-Graduação e Pesquisa em Engenharia, 1992.

[6] Gilberto Alexandre. *Contribuição ao Entendimento da Fluência Não-Drenada*. PhD thesis, COPPE/UFRJ - Instituto Alberto Luiz Coimbra de Pós-Graduação e Pesquisa em Engenharia, 2006.

[7] Gilberto Alexandre. Report on the Viscous Behavior of a Reconstituted Clay in the Oedometric Apparatus. Research report, Saskatchewan Polytechnic, August 2017.

[8] J Brinch Hansen. A model law for simultaneous primary and secondary consolidation. *Proc., 5th Int. Con. on SMFE*, 1:133–136, 1961.

[9] Robert D Holtz and William D Kovacs. *An introduction to geotechnical engineering*, volume 733. Prentice-Hall Englewood Cliffs, 1981.

[10] Laing Barden. Consolidation of clay with non-linear viscosity. *Geotechnique*, 15(4):345–362, 1965.

[11] Jun Kang Chow, Yu-Hsing Wang, Hoi Lun Lui, and Erwin Huang. Determination of consolidation parameters based on the excess pore water pressure measurement using a newly developed u-oedometer. *Acta Geotechnica*, 15(9):2665–2680, 2020.

[12] Hamilton Gray. Progress report on research on the consolidation of fine-grained soils. In *Proceedings, First International Conference on Soil Mechanics and Foundation Engineering*, volume 2, pages 138–141, 1936.

[13] A. S. K. Buisman. Results of long duration settlement tests. In *Proc. 1st ICSMFE*, volume 1, pages 103–107. Cambridge, 1936.

[14] Kwan Yee Lo. Secondary compression of clays. *Journal of the Soil Mechanics and Foundations Division*, 87(4):61–88, 1961.

[15] Alan W Bishop and H. T. Lovenbury. Creep characteristics of two undisturbed clays. *Proc. 7th ICSMFE, Mexico City, 1969*, 1:29–37, 1969.

[16] E Yilmaz and A Saglamer. Secondary and tertiary compression behavior of samsun soft blue clay. In *International Conference on soil mechanics and geotechnical engineering*, pages 329–332, 2001.

[17] Foot R. Ishihara K. Scholesser F. Ladd, C. C. and H. G. Poulos. Stress-deformation and strength characteristics. 1978.